



Particle transport characteristics in the micro-environment near the roadway



Xinming Jin, Lijun Yang*, Xiaoze Du, Yongping Yang

Key Laboratory of Condition Monitoring and Control for Power Plant Equipments of Ministry of Education, School of Energy Power and Mechanical Engineering, North China Electric Power University, Beijing 102206, China

ARTICLE INFO

Article history:

Received 3 January 2016

Received in revised form

21 March 2016

Accepted 22 March 2016

Available online 24 March 2016

Keywords:

Particle transport

Particle concentration

Airflow pattern

Micro-environment

Indoor air quality

Deposition

ABSTRACT

The particles emitted from vehicles will pose a significant threat to the indoor air quality for the buildings next to the road, so it is of benefit to the indoor air quality to reveal the particle transport characteristics in the micro-environment near the roadway. In this work, the particle transport and airflow pattern near a typical highway at various barriers and meteorological conditions are numerically investigated by means of the drift-flux model combined with Eulerian fluid method. The results show that the wind speed plays a significant role in the dispersion of the vehicle emitted particles. The higher the wind speed is, the lower the indoor particle concentration exhibits. The noise barriers can effectively block the incoming flow and restrict the transporting downstream of vehicle emitted particles under most of the meteorological conditions. On the contrary, the vegetation canopies along the roadsides cannot confine the dispersion of the particles. The trees in front of the building facade tend to slow down the air velocity and result in the particle gathering near the windows, which will lead to higher indoor particle concentrations. The indoor particle concentration varies widely with the positions and leaf area density distributions of the trees in the wind direction of 90°, yet, varies little in the wind direction of 45°. The indoor air quality can be improved by increasing the particle deposition velocity on trees and keeping windows closed.

© 2016 Elsevier Ltd. All rights reserved.

1. Introduction

The airborne particles emitted from vehicles will jeopardize human health, causing the diseases such as lung cancer, cardiovascular disease and asthma et al. [1–3]. For the buildings near the highway, the vehicle emitted particles may enter into the indoor environment through the windows, so it is vital to study the particle transport and distribution in the micro-environment near the roadway. Zhang et al. [4,5] investigated the particle number distributions near the roadways, finding that two dilution stages exist after the particles exhaust from the tailpipe, namely, ‘tailpipe-to-road’ and ‘road-to-ambient’, for which the dilution ratios are respectively about 1000:1 and 10:1. Besides, the vehicle induced turbulence plays an important role in mixing the exhaust on the road according to Wang and Zhang [6], which should not be ignored during the pollutant dispersion process near the road.

Roadside barriers, including the noise barriers and trees along the road, can also affect the dispersion of the particles. Steffens et al. [7] numerically investigated the effect of the roadside vegetation barriers on the near-road air pollution, concluding that the particle concentration can be reduced by increasing the leaf area density (LAD). Maher et al. [8] monitored the effect of the trees on the indoor PM₁₀ concentrations, finding that the sparse trees in front of the house can effectively reduce indoor PM₁₀ concentrations as high as 50%. For the noise barriers along the road, a recirculation zone, characterized by strong mixing, was observed to form in the wake of the barrier [9]. Some field experiments in the near road region were also made [10–13].

Although many studies focus on the dispersion of vehicle exhausts, the influence of vehicle emitted particles on the indoor air quality near the roadway is rarely mentioned, and some debates exist on the mitigation effect of the roadside barriers [14–16]. In this study, the indoor air quality in a building near the highway is investigated. The particle transport characteristics for eight kinds of barriers, usually seen in the near road area, are studied under various meteorological conditions.

* Corresponding author.

E-mail address: yanglj@ncepu.edu.cn (L. Yang).

2. Methodology

2.1. Mathematical model

2.1.1. Turbulent airflow model

For the airflow patterns in the micro-environment adjacent to the roadway, the Reynolds averaged Navier–Stokes equations combined with the Renormalization Group (RNG) $k-\epsilon$ model are adopted [17] and the interaction between the particles and fluid has been treated as one-way coupling, since the particle diameters and concentrations of interest are so small that their impacts on the airflow field are negligible [18]. The general form of the governing equations can be expressed as:

$$\nabla \cdot (\rho \vec{u} \varphi) = \nabla \cdot (\Gamma_\varphi \nabla \varphi) + S_\varphi \quad (1)$$

where \vec{u} represents the time-averaged velocity; φ can be regarded as the time-averaged velocity components (u, v, w); turbulent kinetic energy k ; turbulent dissipation rate ϵ or air enthalpy h in different equations; Γ_φ and S_φ are the effective diffusivity and source term for each variable, respectively [19].

A commercial CFD software FLUENT is employed to solve Eq. (1) in the form of discretized algebraic equations with a second-order discretization scheme. The SIMPLE algorithm is applied to couple the pressure and velocity fields. For the buoyancy effect originating from the temperature difference between the indoor and outdoor environments, the Boussinesq approximation is applied [19].

2.1.2. Vegetation model

Plant canopy consists of many leaves and stems that obstruct the incoming air and affect the turbulence characteristics of the air. However, it is impossible to completely reproduce every physical element of the canopy in the model due to the huge computational cost. Instead of characterizing the small leaves and stems, the vegetation has been spatially averaged to produce the average wind speed and turbulence characteristics within the canopy [20]. The solid materials of the leaf and stem are not physically modeled but their effects on the flow are treated as the source or sink terms to the governing equations.

The impediment of the tree canopy to the incoming flow causes some air to move upward and enhances the vertical mixing. On the

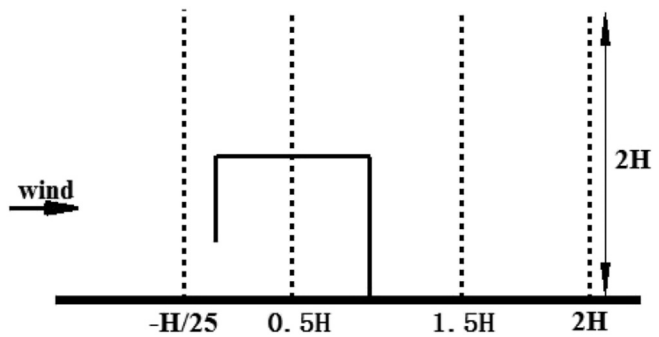


Fig. 2. Locations of four vertical lines on which numerical predictions and experimental measurements are compared.

other hand, the drag force lowers the wind speed and turbulence in the wake of the canopy referred as the windbreak effect [21,22], which may lead to the gathering of the airborne pollutants due to the decrease of the wind speed. For the drag produced by the canopy, the sink term, S_u , given by Thom [23] is used in this study:

$$S_u = -\rho C_D LAD |u| u_i \quad (2)$$

where C_D is the drag coefficient of plants, which is taken as 1.2 according to [10], LAD is the leaf area density and defined as the ratio of the leaf area to the total volume occupied by the vegetative elements, $|u|$ is the wind speed and u_i represents the velocity components.

As air moves through the canopy, the kinetic energy of the flow is converted into the turbulent kinetic energy due to the obstruction of the small leaves and stems. Moreover, this part of turbulence will rapidly dissipate. Thus, the turbulence within the canopy may be high but relatively low behind the canopy [24]. In the equations of the turbulent kinetic energy and dissipation rate, the following source terms developed by Green et al. [25] are added:

$$S_k = \rho C_D LAD (\beta_p |u|^3 - \beta_d |u| k) \quad (3)$$

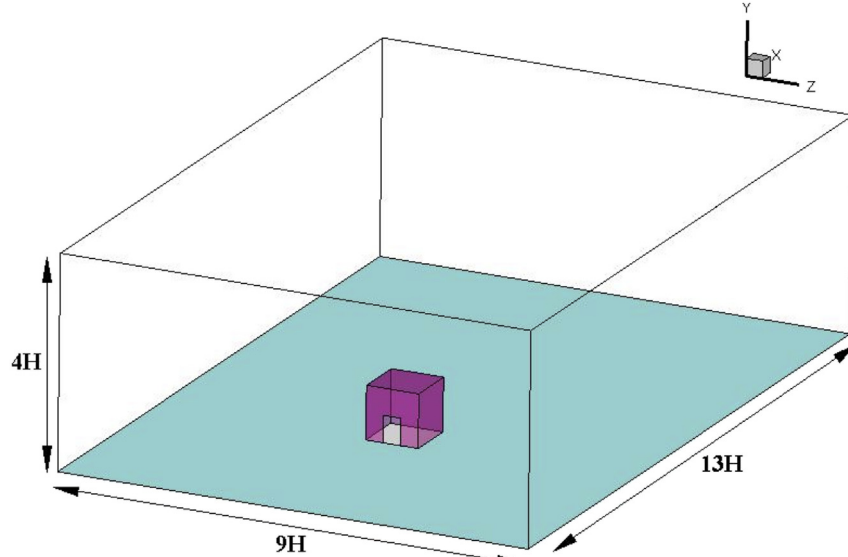


Fig. 1. Computational domain of the validation experiment.

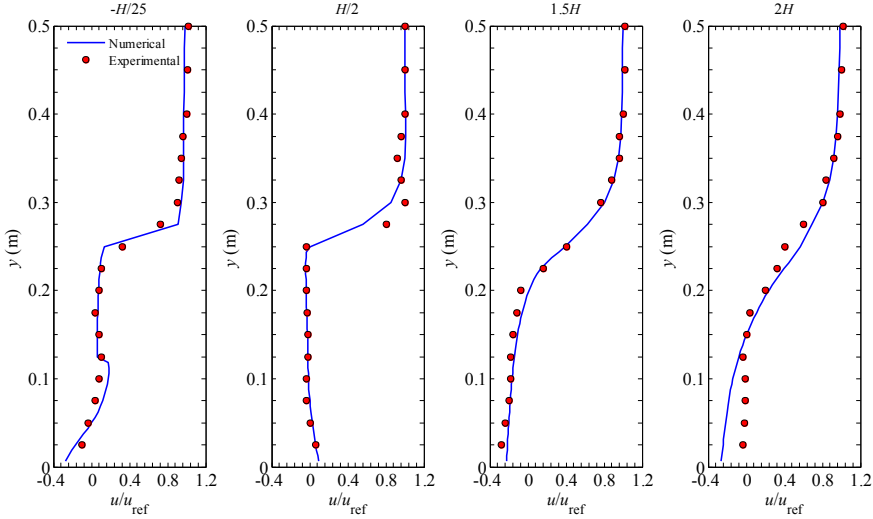


Fig. 3. Comparisons of numerical and experimental normalized velocities on four vertical lines.

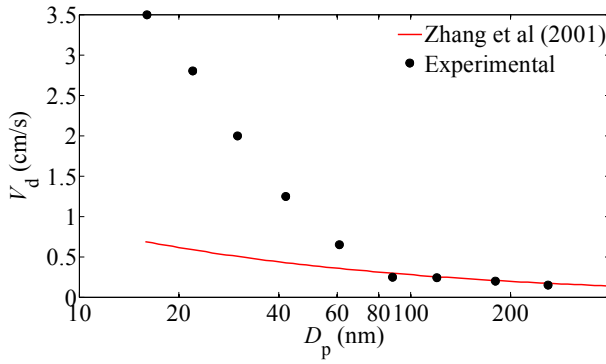


Fig. 4. Comparison between the computed deposition velocities with the model of Zhang et al. [32] and the experimental data in the literature [7].

$$S_e = \rho C_D LAD \left(E_1 \beta_p \frac{\varepsilon}{K} |u|^3 - E_1 \beta_d |u| \varepsilon \right) \quad (4)$$

where the coefficients of β_p , β_d and E_1 are taken respectively as 1, 4 and 1.5 [26].

2.1.3. Particle phase model

The transport and deposition of the particles in micro-environment can be predicted by Lagrangian or Eulerian method [7]. However, a large amount of particle trajectories need to be tracked during the Lagrangian simulation, consuming more computational resources, which has limited its application. In this study, the Eulerian drift-flux model developed by Chen et al. [27] is used to simulate the transport of the particles, which can not only reduce the computational cost but can also characterize the particle distributions more precisely. The governing equation of the particle phase transportation takes the following form:

$$\nabla \cdot \left((\vec{u} + \vec{v}_{s,i}) C_i \right) = \nabla \cdot [(D_i + \varepsilon_p) \nabla C_i] + S_c i \quad (5)$$

where C_i is the particle mass concentration ($\mu\text{g}/\text{m}^3$) of the size group i , $\vec{v}_{s,i}$ is the particle gravitational settling velocity. ε_p the particle eddy diffusivity. In the present simulation, the particle sizes are so small that the assumption of $\varepsilon_p/\mu_t \approx 1$ can be used [28]. $S_c i$ is

the source term. D_i is the Brownian diffusion coefficient with the expression as follows [29]:

$$D_i = \frac{k_B T}{6\pi r_i \eta_a} C_i \quad (6)$$

where k_B is the Boltzmann's constant, T is the Kelvin temperature, r_i is the particle radius, η_a is the molecular viscosity of air and $C_i = 1 + \lambda/r_i \times (A_1 + A_2 \times \exp(-A_3 \times 2 \times r_i/\lambda))$ is the Cunningham correction factor, λ is the mean free path of air and $A_1 = 1.257$, $A_2 = 0.400$, $A_3 = 0.55$. Due to the feasibility of the proposed Eulerian model, the influence of other depositions can be easily incorporated into the model. The dry deposition model for the particles is introduced below.

2.1.4. Dry deposition model

When the particle is intercepted within the canopy, it is regarded as being removed from the air and depositing on the vegetative surfaces. Owing to the space averaging method adopted in this work, a statistical deposition model should be employed. Many dry deposition models of atmospheric particles were adopted in the multi-scale air quality prediction [30,31]. In the current work, the deposition model developed by Zhang et al [32], is used, in which the deposition processes, such as the turbulent transfer, Brownian diffusion, impaction, interception, gravitational settling and the particle rebound, have all been taken into account. The particle deposition rate is computed as:

$$\frac{\partial C_i}{\partial t} = S_c i = -LAD v_d C_i \quad (7)$$

with v_d being the deposition velocity computed by the dry deposition model, C_i the particle concentration inside the canopy.

2.1.5. Particle resuspension

The particles deposited on the canopy may be absorbed into the tree, while most of them are retained on the surfaces, which may re-enter into the atmosphere via resuspension, especially for the larger ones. For particles with the diameter of 2.5 μm , Nowak et al. [33] gave the resuspension percentages at different wind speeds, according to which a quadratic curve is fitted in this work. Because the maximum wind speed in this paper is smaller than 10 m/s, the resuspension percentages from 0 to 13% are employed. Finally, the

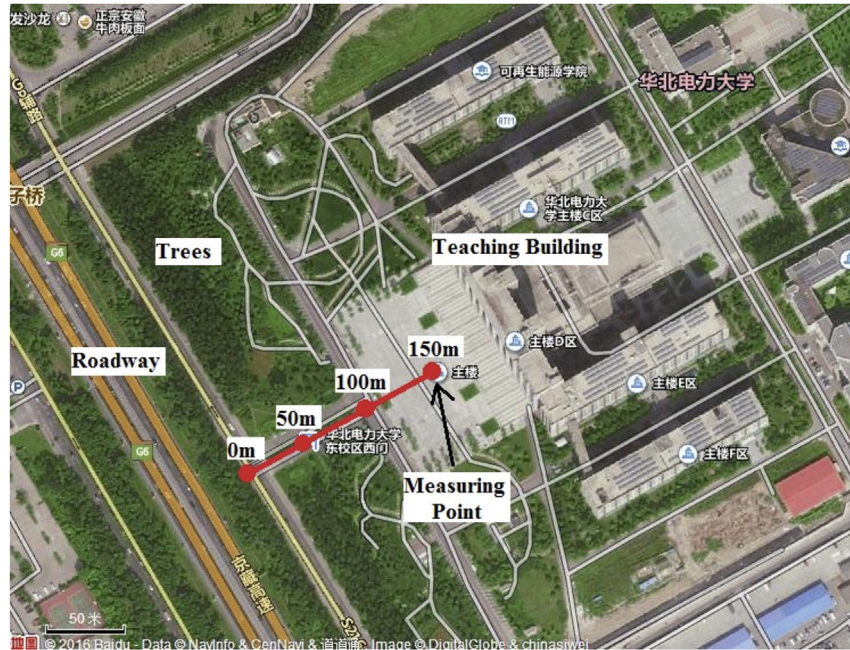


Fig. 5. Aerial view of the experimental spot for the particle transportation measurement near the typical expressway.

quadratic fitting curve is $P_{\text{resuspension}} = (-0.041v^2 + 1.7v - 0.16)/100$, where $P_{\text{resuspension}}$ represents the percentage of resuspension and v is the wind speed. Owing to the small size, the resuspension process for $0.1 \mu\text{m}$ is ignored. The resuspension percentage for $10 \mu\text{m}$ is assumed to be identical to that for $2.5 \mu\text{m}$ in this study.

2.2. Model validation

2.2.1. Air flow around a bluff body

Jiang et al. [34] investigated the airflow pattern around an isothermal scaled room by a wind tunnel test. The dimension of the room is $L(x) \times H(y) \times W(z) = 250 \text{ mm} \times 250 \text{ mm} \times 250 \text{ mm}$, as shown in Fig. 1, with the wall thickness of 6 mm. In the experiment, the mean air velocity and its fluctuation along 10 vertical lines at the middle plane in the z direction were measured with the laser Doppler anemometer. Four lines shown in Fig. 2 are chosen to compare the numerical predictions with the experimental results. The geometry of the computational domain is $x \times y \times z = 13H \times 4H \times 9H$, the inlet velocity profile in the x

direction follows $u_y = (u_0/\kappa)\ln(y/y_0)$ and the velocity components in other directions are zero. The Renormalization Group (RNG) $k-\epsilon$ model combined with wall functions are used to compute the turbulence in the domain. The comparisons between the experimental measurements and simulation results are shown in Fig. 3. It can be observed that, although the simulation results at the upper part of the line $H/2$ and lower part of the line $2H$ present little deviations from the measurements, the overall performance of the present numerical model is satisfactory, which justifies the application of the RNG $k-\epsilon$ model in this study.

2.2.2. Particle deposition velocity inside trees

It should be noted that the deposition model mentioned above is developed originally for large scale air quality predictions, and applicable for the deposition velocity calculation over a forest, which has been validated against the field data. Whereas, the vegetation barriers in this study are only a row of trees, the deposition models or field experiments for an isolated tree or a small number of trees are rarely seen. Some indirect measurements about

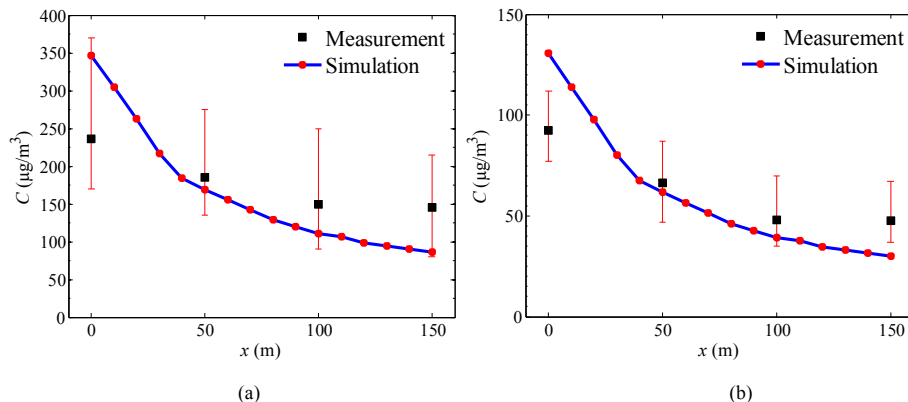


Fig. 6. Comparisons between the measured particle concentrations and simulated ones in 90° wind direction, 1 m/s wind speed and dense tree canopies planted along the roadside. (a) PM_{10} , (b) $\text{PM}_{2.5}$.

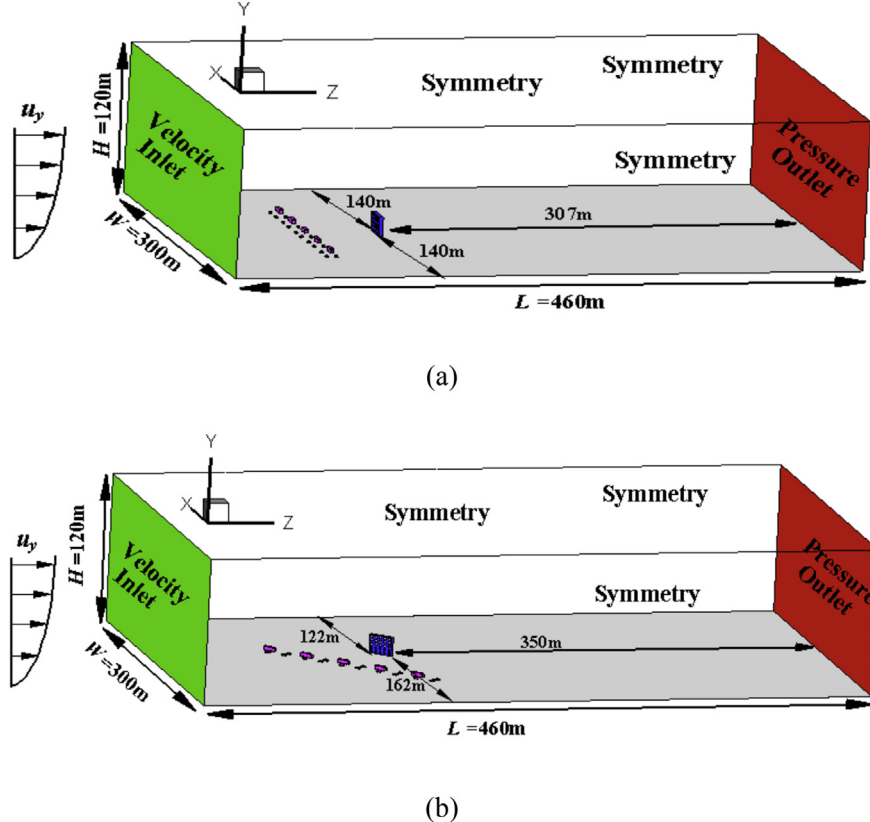


Fig. 7. Dimensions and boundary conditions of the computational domains in two wind directions. (a) 90° inflow, (b) 45° inflow.

the particle deposition on a row of trees have been carried out. Steffens et al. [7] measured the particle number concentrations near a highway with the isolated tree canopy on the roadside. Derived from the measured particle concentrations, the deposition velocities within the canopy have been calculated and compared with the prediction results from the model of Zhang et al. [32] as shown in Fig. 4. It can be seen that for the particles smaller than 80 nm, the deposition velocities predicted by the model are conspicuously lower than those from the indirect measurement. For the particles larger than 80 nm, however, the model predicted velocities match highly with the experimental results. Although the number of ultrafine particles in the vehicle exhaust is relatively large, the ultrafine particles will grow by condensation and shrink by evaporation. Moreover, the processes of nucleation and coagulation can also change the ultrafine particle size distributions. In order to accurately predict the evolution of ultrafine particles, the population balance equation (PBM) should be solved, which is a significant subject in our future work. In this paper, the particles with aerodynamic diameters ranging from 0.1 μm to 10 μm are of interest, for which the influences of aerosol dynamics (condensation, evaporation, coagulation and nucleation) are negligible and the emission of fine particles from the roadway is also a major source for the urban air pollution. As seen in Fig. 4, the large scale deposition model works fairly well for the particles larger than 0.1 μm , so the model developed by Zhang et al. [32] is applied to the prediction of particle deposition velocities.

2.2.3. Comparison with field measurements

To investigate the particle transport characteristics near the roadway, an on-site measurement was carried on near a typical expressway in China by Li et al. [35]. The aerial view of the

experimental spot is shown in Fig. 5, in which the roadway is parallel with the building and the trees are planted along the curb of the road. During the measurements, four positions of 0 m, 50 m, 100 m and 150 m away from the road curb were selected to place the Portable Aerosol Spectrometer GRIMM 1.109, which is used to measure the mass concentrations of PM₁₀ and PM_{2.5}. From April 18 to May 21 in 2015, the variations of particle concentrations at 8:00–11:00am and 14:00–17:00pm in each day were recorded. The wind speeds during the measurement vary from 0.3 to 2.5 m/s according to the data provided by the Chinese Meteorological Administration in Changping District of Beijing. The particle concentration distributions in the wind direction perpendicular to the roadway are employed to compare with the simulation results, as shown in Fig. 6.

The results show that the simulated particle concentrations near the curb are relatively higher than the measurement, which can be attributed to the particle deposition on the grassland located along the points of measurement. Furthermore, the roadside trees in the real scenario are denser than those of the model and the real wind speeds are relatively smaller, restraining the particle dispersion from the roadway. However, the overall changing trends of the simulation results are consistent with the measurement, showing an exponential variation as indicated in many investigations, which further justifies the application of the numerical model in this work. It should be noted that the emission sources of PM₁₀ and PM_{2.5} used in this study are the same, namely $Q = 6375 \text{ mg/s}$. However, the sources are 425 mg/s for PM₁₀ and 160 mg/s for PM_{2.5} in the field scenarios owing to the lower traffic volume. Whereas the modeling and numerical methods adopted in this work are completely same as those taken in the experimental validation.

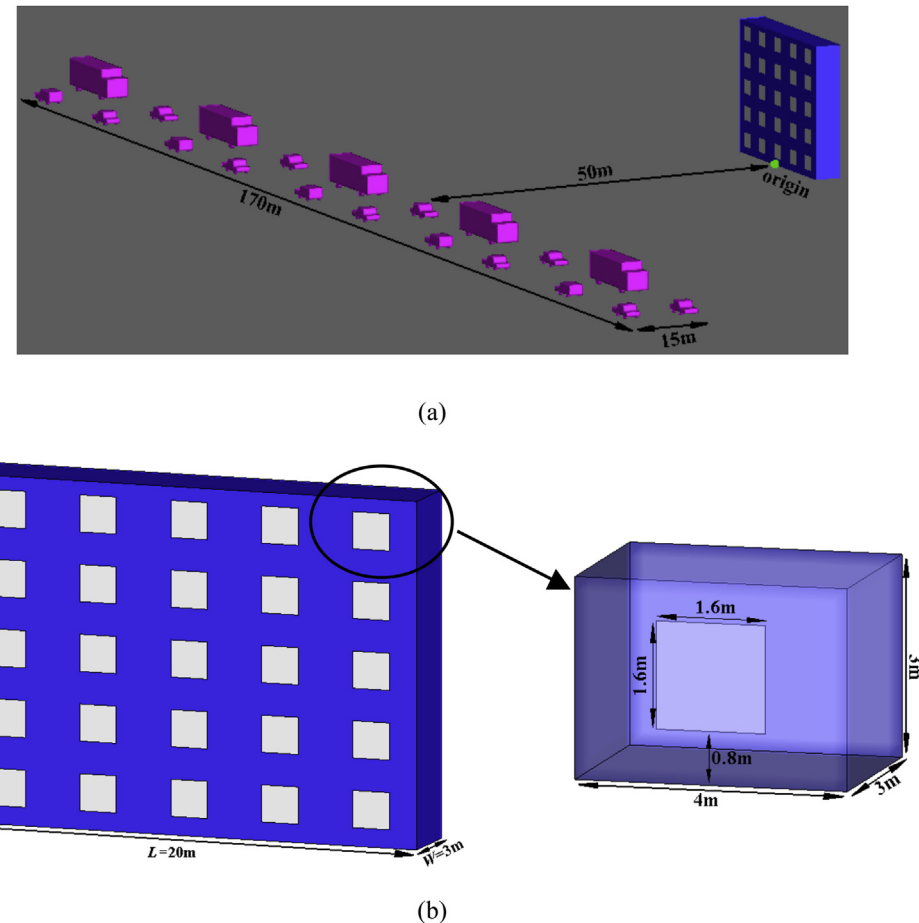


Fig. 8. Geometries of (a) the road and (b) the building.

2.3. Numerical case description

To investigate the impact of the vehicle emitted particles on the indoor air quality, a typical building near the highway usually seen in Beijing has been selected and the computational domains are shown in Fig. 7 with the dimension of $L \times W \times H = 460 \text{ m} \times 300 \text{ m} \times 120 \text{ m}$, which is large enough to eliminate the impacts of the domain boundaries on the flow field. Besides, two inflow directions of 90° and 45° are analyzed. In the direction of 90° , the building is 140 m away from the lateral surfaces and 307 m from the outlet as shown in Fig. 7(a). Similarly, the location of the building in the wind direction of 45° is given in Fig. 7(b), where all the distances from the domain boundaries in the x , y and z directions comply with the CFD simulation requirements recommended by COST Action 732 [36].

The detailed geometries of the building and road are presented in Fig. 8, in which the size of the road is $\text{length} \times \text{width} = 170 \text{ m} \times 15 \text{ m}$ with two rows of running vehicles. The vehicles are composed of two categories, the larger diesel trucks and the smaller gasoline cars. The spacing between two vehicles is bigger than 10 m [37], and the speeds of the vehicles are all set as 148 km/h [38]. The building is parallel with the road and 50 m away from the curbside as shown in Fig. 8(a). Fig. 8(b) shows a typical five-floor building containing 25 rooms of interest. The geometric size of a single room is $\text{length} \times \text{width} \times \text{height} = 4 \text{ m} \times 3 \text{ m} \times 3 \text{ m}$ with a window located at the middle of the front surface and 0.8 m higher than the room floor. The size of the window is $\text{length} \times \text{width} = 1.6 \text{ m} \times 1.6 \text{ m}$.

Some cases analogous to the real scenarios of the tree canopies and noise barriers in reducing the airborne particles are studied. For the region near the building, two positions of the tree canopy, respectively 10 m and 20 m from the building facade, are considered. The dimension of the canopy is $\text{length} \times \text{width} \times \text{height} = 60 \text{ m} \times 4 \text{ m} \times 8 \text{ m}$ and 2 m higher than the ground, so the height of the tree is 10 m, representing a relatively tall species. Besides the canopies located in the building adjacent area, the vegetation and noise barriers near the road are also taken into account. The noise barriers are built along the both curbsides of the road with $\text{height} \times \text{width} = 4 \text{ m} \times 1 \text{ m}$ as indicated in Fig. 9(b). The geometry for each of the roadside canopies is assumed to be $\text{length} \times \text{width} \times \text{height} = 170 \text{ m} \times 4 \text{ m} \times 4 \text{ m}$ and 2 m higher than the ground, implying the height of the tree is 6 m frequently seen in urban environment. About 4 million grid cells are utilized to discretize the computational domain with fine meshes in the near-vehicle and building adjacent regions and coarse meshes in the outer regions by reducing the grid interval exponentially.

The windward surface of the computational domain is defined as the velocity inlet boundary condition. For the urban environment, the typical wind speed following a power law equation is adopted here [39]:

$$u_y = 0.35 u_w y^{0.25} \quad (8)$$

where u_w is the wind speed measured at 10 m above the ground and y is the vertical distance. Two wind profiles with $u_w = 1 \text{ m/s}$,

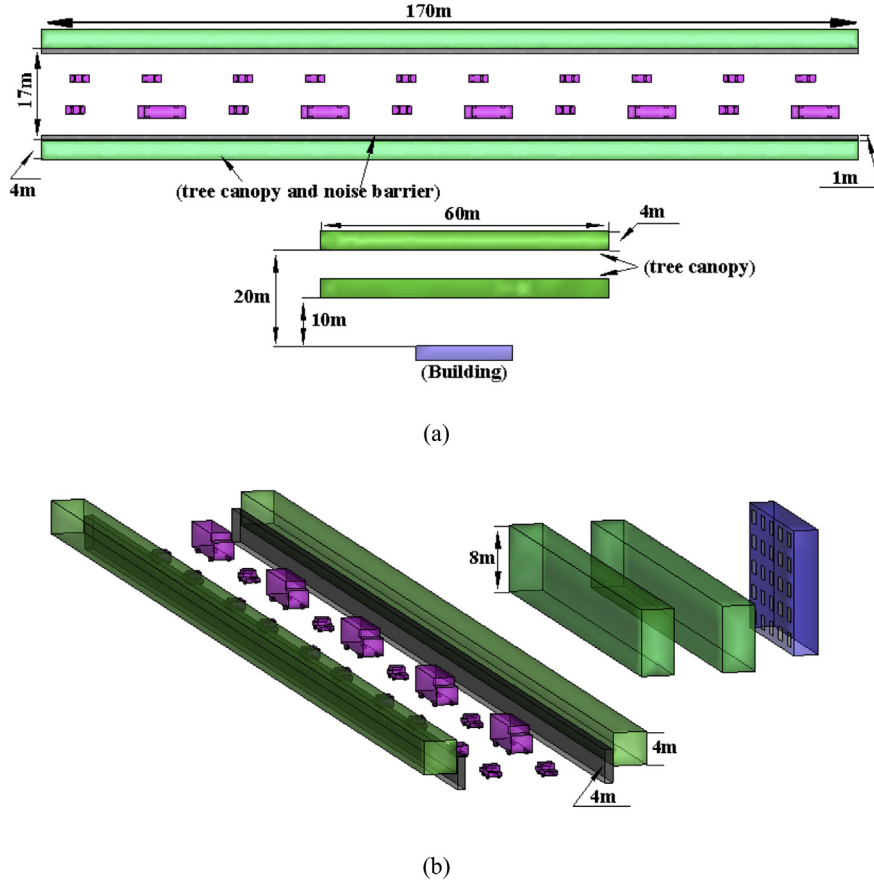


Fig. 9. Schematics of the dimensions for the barriers. (a) top view, (b) oblique view.

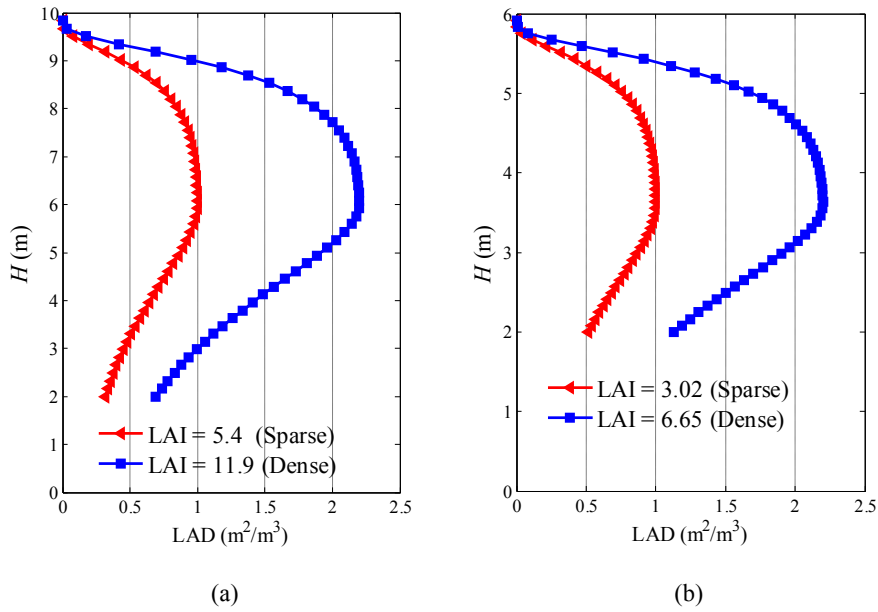


Fig. 10. Leaf area density (LAD) distributions for the canopies (a) next to the building and (b) along the roadsides.

and 4 m/s are considered in this work [40]. For the turbulence boundary conditions, the turbulence intensity and length scale are specified, which are 8% and 1 m respectively as an illustrative case [40]. The outlet surface is set as the pressure outlet condition and

the lateral and upper surfaces of the domain are symmetrical as shown in Fig. 7.

Previous investigations have confirmed the effectiveness of natural ventilation in improving indoor air quality [41]. While in

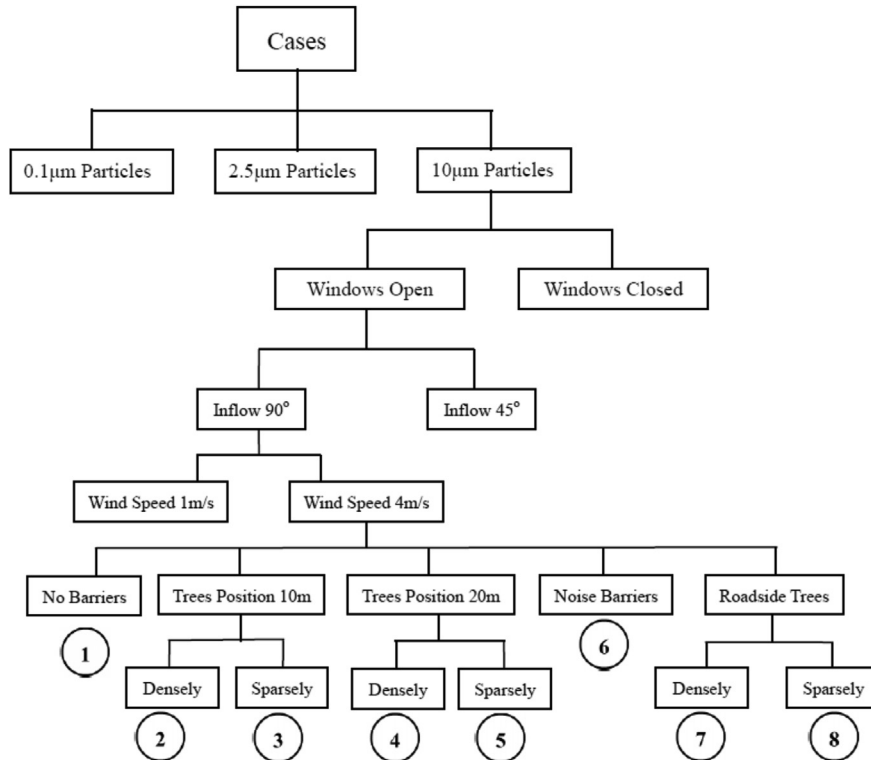


Fig. 11. Overview of the simulation cases in this study.

densely inhabited cities, a small room may only have one external facade [40], which leads to the wide application of single-sided natural ventilation. In this study, the windows are firstly kept open to mimic the single-sided natural ventilation, and then closed to analyze the effect of windows on the outdoor particle infiltration. When the windows are open, the temperature difference between the indoor and outdoor environments can greatly affect the transport of the airborne particles [42]. Therefore, the Boussinesq approximation is used to consider the buoyancy effect, for which the temperature of the atmospheric environment is set as 293 K, while the temperatures of the room wall surfaces are 298 K recommended by Gao et al. [40].

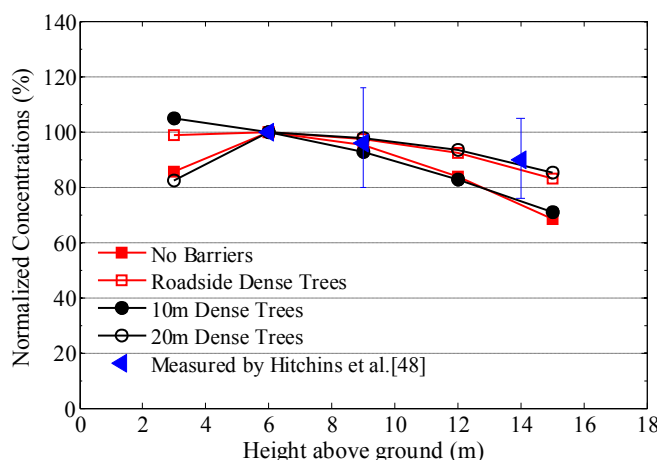
To obtain the particle transport characteristics with different barriers, an Eulerian drift-flux model considering gravitational settling is employed [28]. A mixing zone above the road is created to act as the source of the vehicle emitted particles. Determined by the quantity proportion of the heavy-duty diesel trucks, the height of the mixing zone is taken as 2.5 m according to Wang and Zhang [6]. The transport of particles with three diameters, namely 10 μm, 2.5 μm and 0.1 μm, are simulated, which represent respectively large, small and ultrafine categories. The emission rate is calculated from the traffic volume, about 15937 vehicles per unit hour, and the particle emission factors which are different for the three categories. For the sake of simplicity, a uniform emission factor, 9.72 mg/km according to Shen et al. [43], is adopted. As a result, the emission rate Q is 6375 mg/s for each category. The particle concentrations are basically normalized as follows [44]:

$$c^+ = \frac{cu_H H}{Q/l} \quad (9)$$

where c is the particle concentration, u_H is taken as 2.5 m/s, $H = 15$ m is the height of the building and $l = 170$ m is the length of the emission source.

The leaf area density (LAD) of the tree canopies as a function of height is a key issue to the particle transportation. The empirical relationship developed by Lalic and Mihailovic [45] has been validated by many field data and used to describe the profile of the LAD as follows:

$$\begin{aligned} \text{LAD} &= L_m \left(\frac{h - z_m}{h - z} \right) \exp \left[n \left(1 - \frac{h - z_m}{h - z} \right) \right] \\ n &= \begin{cases} 6, & 0 \leq z < z_m \\ \frac{1}{2}, & z_m \leq z \leq h \end{cases} \end{aligned} \quad (10)$$

Fig. 12. Comparison of normalized concentration profiles for $\text{PM}_{0.1}$ among four simulated cases and the measurements by Hitchins et al. [48] with windows closed, at the wind speed of 1 m/s and in the perpendicular wind direction.

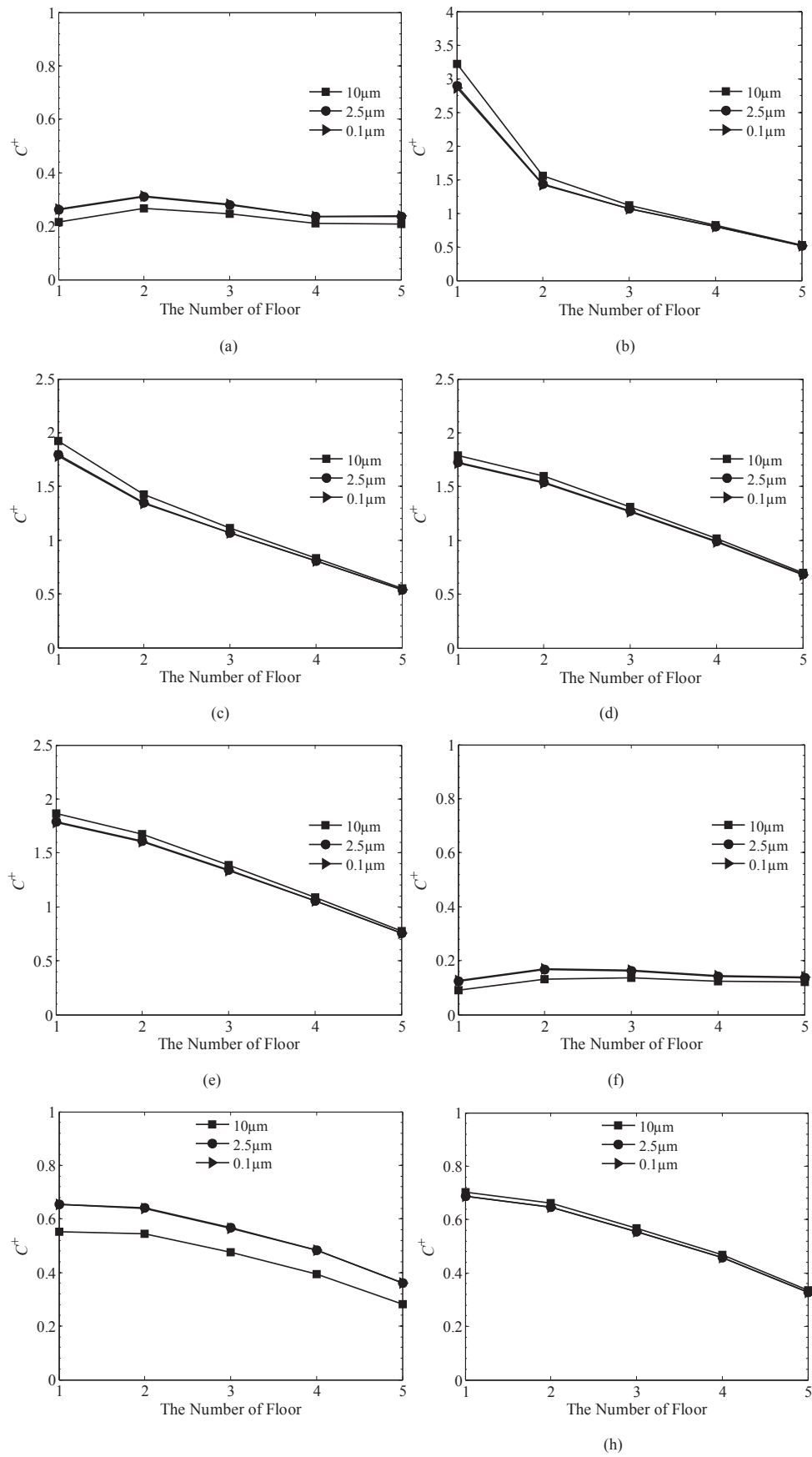


Fig. 13. Comparisons of the indoor particle concentrations with windows open for three particle categories and eight kinds of barriers in 90° inflow direction and at wind speed of 4 m/s. (a) no barriers, (b) 10 m dense trees, (c) 10 m sparse trees, (d) 20 m dense trees, (e) 20 m sparse trees, (f) noise barriers, (g) roadside dense trees and (h) roadside sparse trees.

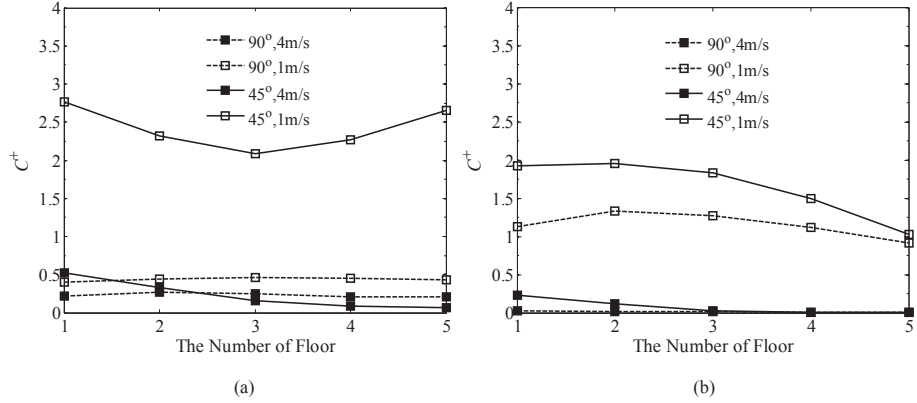


Fig. 14. Indoor particle concentration profiles with no barriers. (a) windows open, (b) windows closed.

with L_m being the maximum LAD and z_m the location at which the maximum LAD occurs. h is the height of the tree and z is the location where the LAD is calculated. In this work, the value of z_m is taken as $0.6 h$ [7]. L_m can be obtained from the leaf area index (LAI), which is used to measure the ratio of the leaf surface area to the ground surface area and relates to the LAD as follows:

$$\text{LAI} = \int_0^h \text{LAD} dz \quad (11)$$

For each position of the trees in front of the building, two kinds of LAD distributions of dense and sparse, corresponding respectively to $\text{LAI} = 11.9$ and 5.4 , are investigated. Similarly, the densely and sparsely planted canopies along the roadside are also considered with the LAI equal respectively to 6.65 and 3.02 . By

numerically integrating Eq. (11), the L_m can be obtained and the profiles of the LAD are shown in Fig. 10.

When the particles are intercepted by the vegetative elements, the particles are treated as deposited. The particle deposition flux, $J_{d,i}$, is used to obtain the particle removal capability of the canopy [28]:

$$J_{d,i} = v_{d,i} C_{b,i}^+ \quad (12)$$

where $C_{b,i}^+$ is the dimensionless concentration of the particles in the cell within the canopy. $v_{d,i}$ is the deposition velocity of the particle. For the three categories of the particles, $10 \mu\text{m}$, $2.5 \mu\text{m}$ and $0.1 \mu\text{m}$, the corresponding deposition velocities calculated with the model of Zhang et al. [32] are respectively 2.5 mm/s , 0.5 mm/s and 2 mm/s .

Three categories of particles, two states of the windows, two wind directions and two wind velocity profiles have been

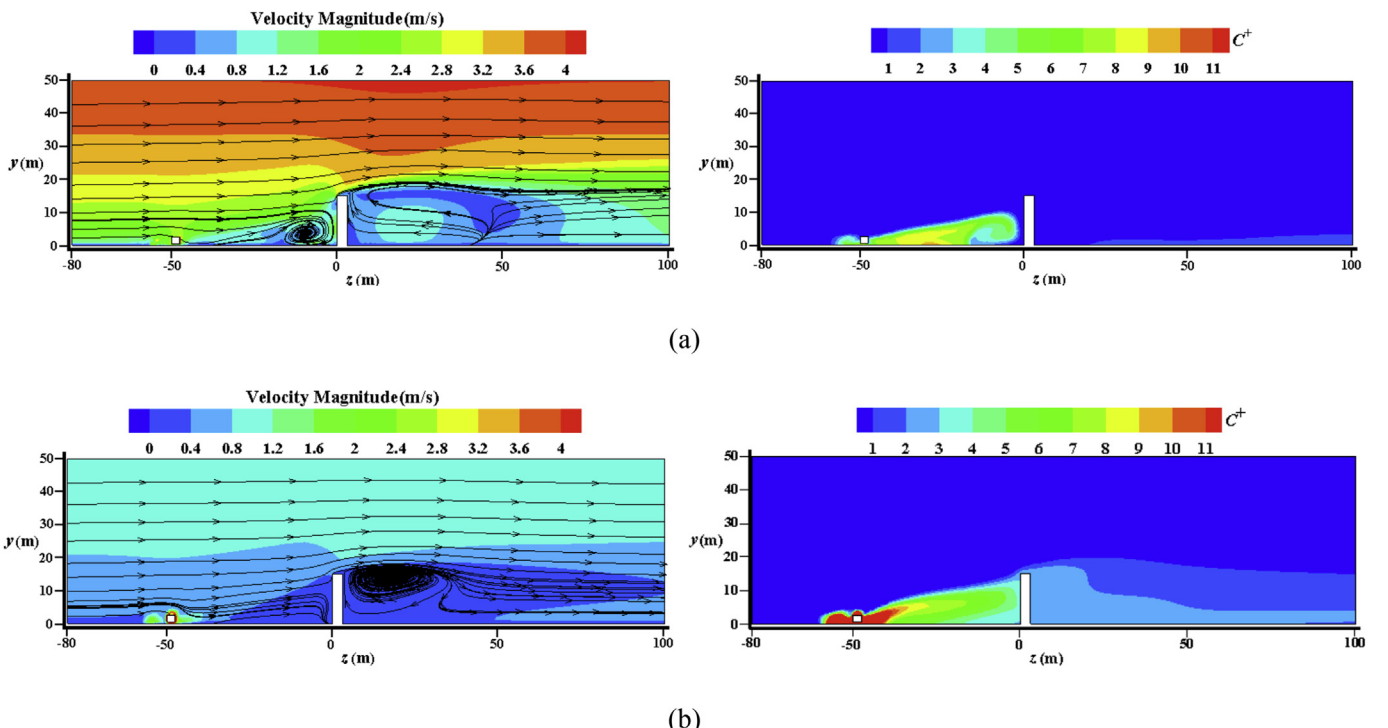


Fig. 15. Airflow fields and corresponding particle concentration distributions on the plane of $x = 0 \text{ m}$ at two wind speeds of (a) 4 m/s and (b) 1 m/s in the wind direction 90° , for the scenario of no barriers with windows closed.

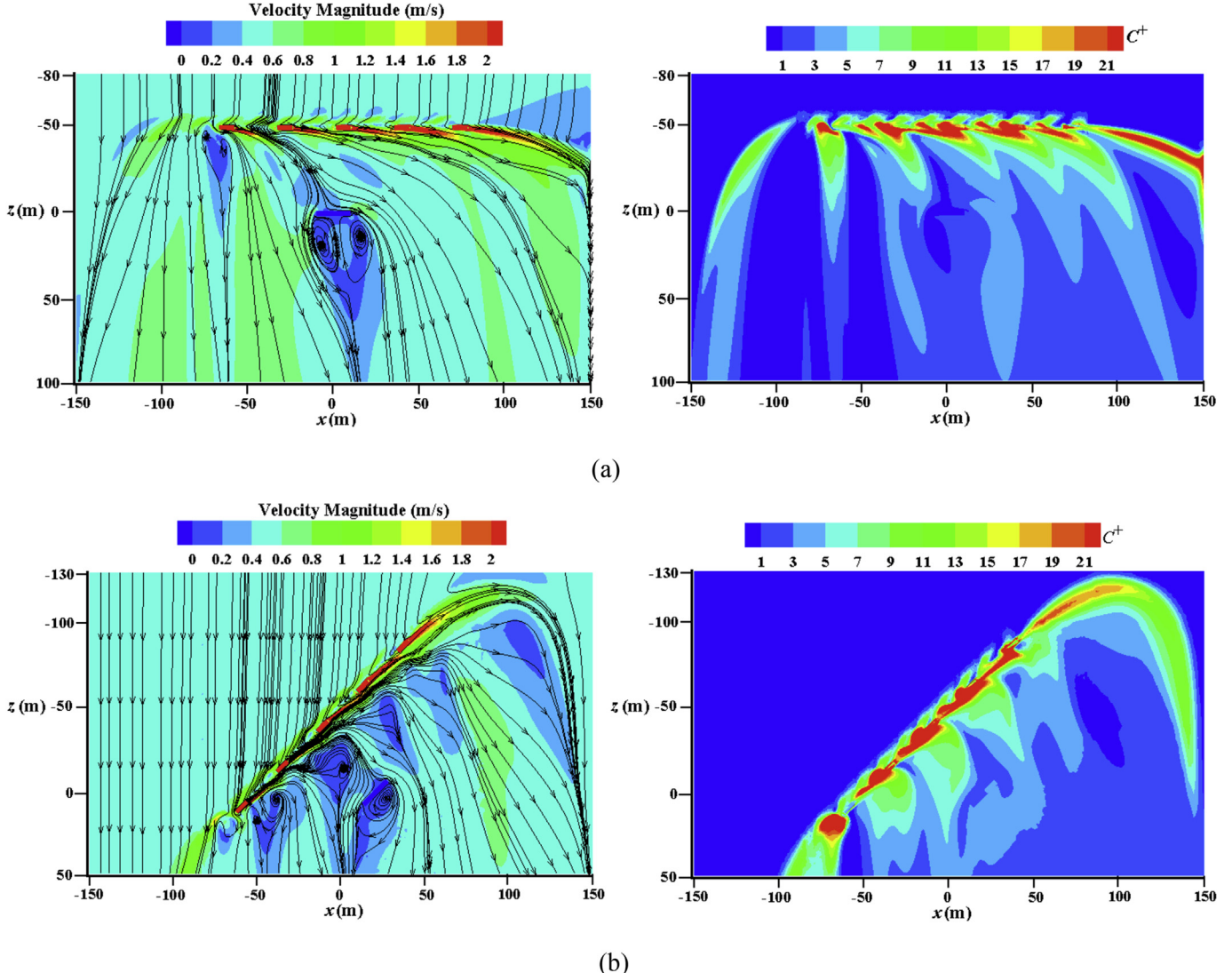


Fig. 16. Airflow fields and corresponding particle concentration distributions on the plane of $y = 3$ m in two wind directions of (a) 90° and (b) 45° at the wind speed 1 m/s, for the scenario of no barriers with windows open.

calculated as indicated in Fig. 11. For each case, eight kinds of barriers as marked with the circled number are considered, and then altogether $24 \times 8 = 192$ cases are simulated in this study.

With the windows open, the outdoor airborne particles can directly enter into the indoor environment. The mean concentrations in five rooms of each floor are recorded to represent the indoor air quality. While the outdoor particles can only enter into the room by infiltration process and most particles are blocked outside as the windows closed. According to Chen and Zhao [46], the infiltration factor, F_{in} , depends on the size of the particles. For large particles, they are easy to be intercepted by the cracks and crevices in the building envelope, so the infiltration factor is low. Whereas, the ultrafine particles smaller than the cracks are difficult to be blocked, which leads to a high infiltration factor nearly to 1.0. The infiltration factors proposed by different work vary in the large range of 0.3–0.82 for $PM_{2.5}$, 0.17–0.52 for PM_{10} . For the ultrafine particles ($PM_{0.1}$), the range of 0.68–0.92 was reported by Kearney et al. [47]. It should be noted that the indoor particle concentration varies widely with the infiltration factor. For the convenience of comparison, the median values for different particles are chosen to represent the infiltration of outdoor particles, namely 0.35 for PM_{10} ,

0.56 for $PM_{2.5}$ and 0.80 for $PM_{0.1}$. The relationship between the indoor and outdoor particle concentrations can be expressed as:

$$C_{in} = F_{in}C_{out} + C_S \quad (13)$$

where C_{in} is the indoor particle concentration, C_{out} is the outdoor particle concentration and C_S is the concentration of indoor particle sources which is neglected in this study. The C_{out} is assumed equal to the particle concentration adjacent to the windows.

In the process of calculation, the steady state airflow pattern is obtained by solving RANS equations with the solver FLUENT, then the drift-flux model is incorporated by the user defined scalar (UDS) module to compute the particle distributions. For all variables, the convergence criteria are set as 10^{-6} based on the scaled residual. Besides, the area-weight average velocity magnitudes at several interior faces in the domain are also monitored. After about 5000 iterations, the residuals and average velocities maintain at an acceptable level, then the solutions are regarded as converged.

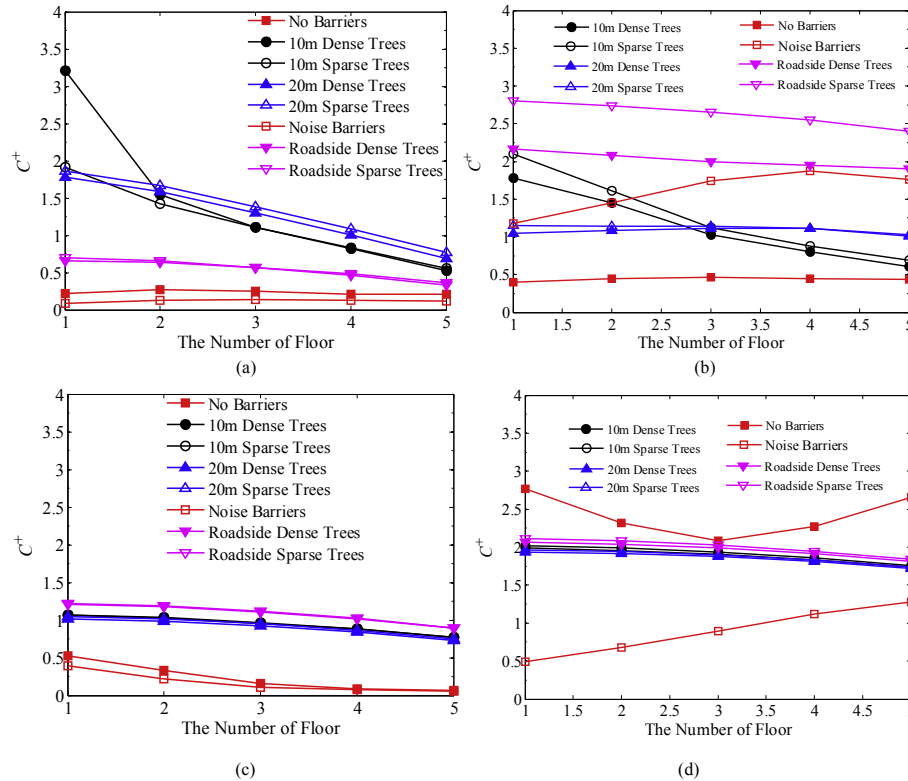


Fig. 17. Indoor particle concentration profiles with windows open for eight kinds of barriers under different wind directions and speeds. (a) 90° inflow and 4 m/s wind speed, (b) 90° inflow and 1 m/s wind speed, (c) 45° inflow and 4 m/s wind speed, and (d) 45° inflow and 1 m/s wind speed.

3. Results and discussion

3.1. Transport characteristics of different particle categories

Hitchins et al. [48] did an on-site measurement about the dispersion of the particles from vehicle emissions around high-rise buildings, in which the ultrafine particle concentrations at different heights of the building envelope were recorded. During the measurement, the wind speed was approximately 1 m/s and the wind direction was perpendicular to the roadway and the building facade. Fig. 12 shows the normalized concentration profiles for PM_{0.1} based on the value at the height of 6 m for four numerical cases and the measurement data from Hitchins et al. [48]. It can be seen that although the building locations are not completely the same, the general changing trends are similar to each other, that is, the particle concentrations decrease as the height increases. What's more, the numerical results are consistent with the measured data, showing that the performance of the numerical model is fairly well to predict the particle transport characteristics.

Fig. 13 shows the indoor particle concentrations with windows open for three particle categories and eight kinds of barriers (no barriers, 10 m dense trees, 10 m sparse trees, 20 m dense trees, 20 m sparse trees, noise barriers, roadside dense trees and roadside sparse trees) in the 90° inflow direction and at the wind speed of 4 m/s. At a large wind speed, the inertial effect dominates the particle transport process. It can be seen that the differences between 2.5 μm and 0.1 μm are negligible, for which the gravitational effect is relatively weak. However, the relatively large difference is presented for the category of 10 μm. In addition, the mean concentrations of 10 μm particles for three kinds of barriers, namely, no barriers (barrier 1), the noise barriers (barrier 6) and the roadside dense trees (barrier 7), are all smaller than the other two categories

of the particles, which could be attributed to the gravity effect. After emission from the tailpipes, the particles on the road will be advected to the downstream by the airflow. For the scenarios with no barriers, small particles follow the air movement tightly with longer transport distances, however, the distances for big particles become shorter owing to the gravitational force, which leads to a small mean concentration for 10 μm particles. As for the noise barriers and dense canopies along the road, the incoming flow will be blocked, resulting in more particles gathering in the roadside. As a result, large particles tend to be confined while most of the smaller ones will transport downstream. It can also be seen that the concentration difference between the large and small particles is reduced with ascending the building floor, implying that the small particles are also difficult to diffuse to a certain height even with a weak gravity effect.

Although the indoor concentrations of 10 μm particles vary widely with those of 2.5 μm and 0.1 μm in some floors, the changing trends of the mean concentration profiles with the building floors are similar among the three categories of particles. Moreover, similar profiles among the three particles are also presented under other meteorological conditions. Therefore, the following discussions will only focus on the category of 10 μm, and the concluding remarks can be applied to other particle sizes.

3.2. Particle distributions with no barriers

The scenarios of no barriers have been treated as the benchmark, against which the particle concentrations of other kinds of barriers in the same wind direction and at the same wind speed are compared. The mean indoor concentration profiles of 10 μm particles with no barriers are shown in Fig. 14. Generally, the wind speed and direction play important roles in the distributions of the

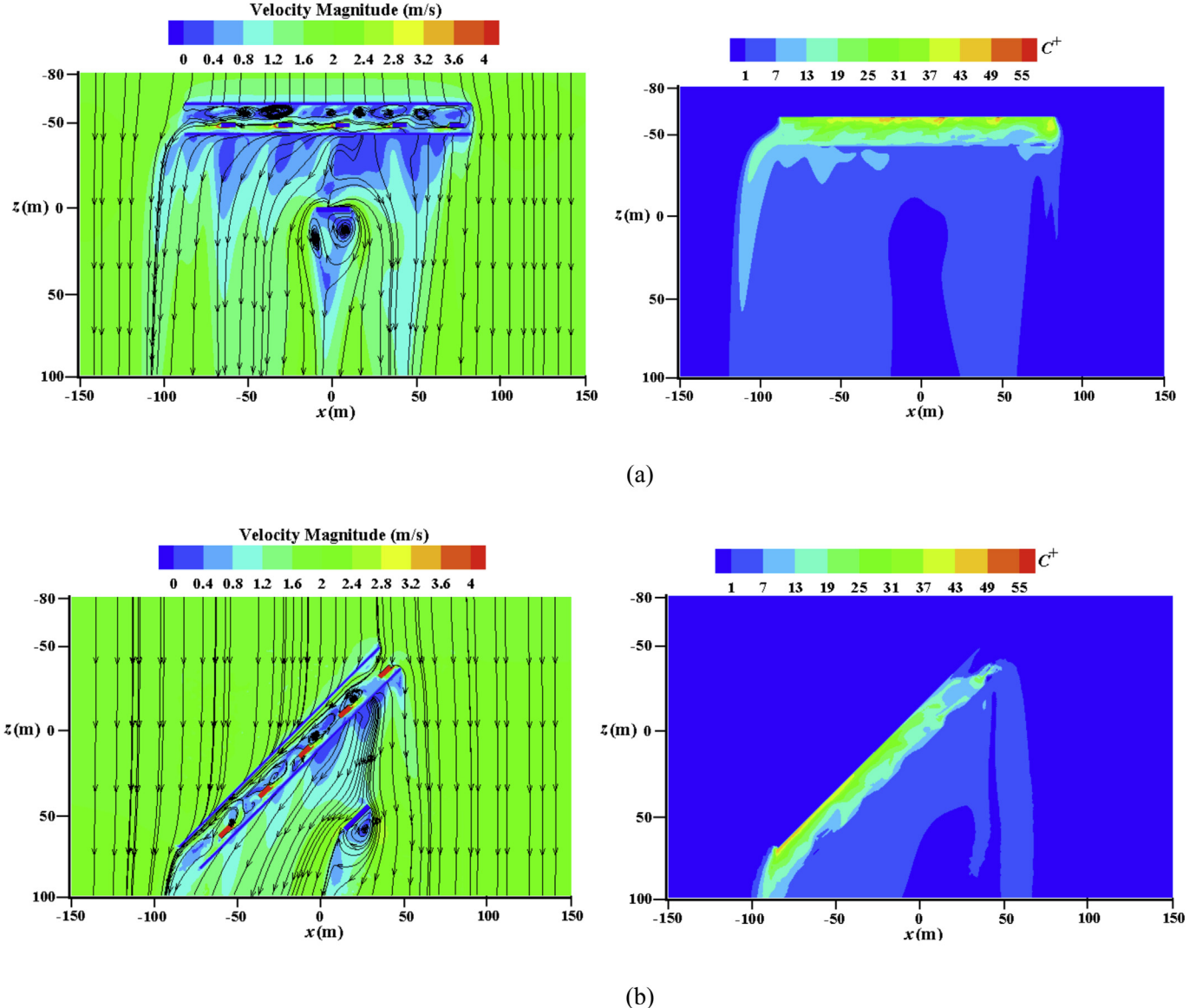


Fig. 18. Airflow fields and corresponding particle concentration distributions on the plane of $y = 3$ m in two wind directions of (a) 90° and (b) 45° at the wind speed 4 m/s, for the scenario of the noise barriers with windows open.

indoor particle concentrations. In the same wind direction, the larger the wind speed is, the lower the indoor concentration exhibits. As shown in Fig. 15, the airflow patterns and corresponding particle concentration distributions on the plane of $x = 0$ m at two wind speeds of 4 m/s and 1 m/s in the 90° wind direction with the windows closed are illustrated. At the high wind speed, a large vortex generates in front of the building, which can gather the particles. However, the air velocity at the facade of the building is relatively high that can transport most of particles away from the windows. On the contrary, at the wind speed of 1 m/s the air velocity in front of the building is low and more particles tend to accumulate near the windows.

Fig. 16 gives the airflow fields and corresponding particle concentration distributions on the plane of $y = 3$ m in two wind directions of 90° and 45° at the wind speed of 1 m/s, when the windows are open. According to the work of Wang and Zhang [6], the interaction between the vehicles and ambient air can induce the turbulence, which enhances the mixing process of the exhausts

and makes the on-road airflow fields more irregular. In the 90° wind direction, most of incoming air can flow through the interval between two vehicles and the air velocity behind the road is relatively high, which is beneficial to the particle dispersion. When the inflow direction is 45° , the interval between the vehicles becomes shorter, obstructing the air traversing, which lowers the air velocity behind the road and results in more particles gathering around the building. It shows that for the no barriers cases, the oblique wind direction and the lower wind speed will lead to higher indoor particle concentrations as shown in Fig. 14.

3.3. Particle transport characteristics with windows open

Fig. 17 shows the particle mean concentrations in each floor with windows open at two wind speeds in two wind directions. Except for the 90° wind direction and wind speed of 1 m/s, the noise barriers can effectively restrain the transport of the vehicle emitted particles to the indoor environment in all other scenarios.

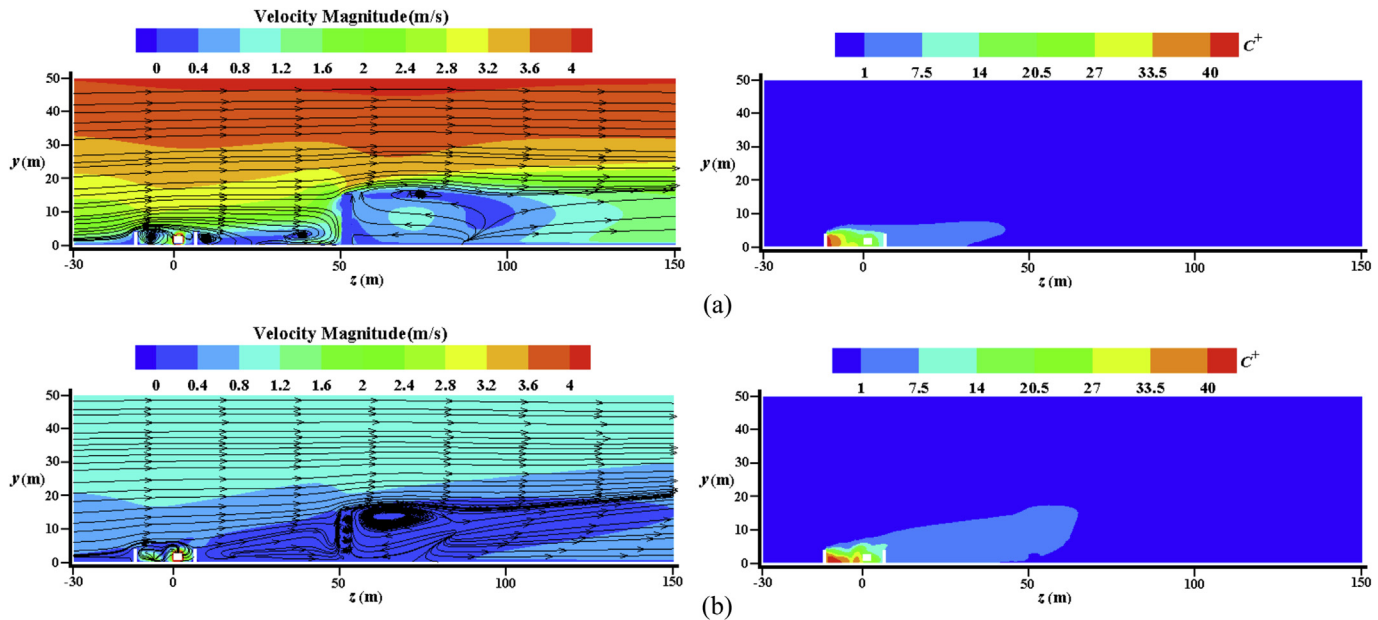


Fig. 19. Airflow fields and particle concentration distributions on the plane of $x = 0$ m at two wind speeds of (a) 4 m/s and (b) 1 m/s in the wind direction 90° , for the scenario of the noise barriers with windows open.

The airflow patterns and corresponding particle concentration distributions with the noise barriers on the plane of $y = 3$ m at the wind speed of 4 m/s in two wind directions are given in Fig. 18. The noise barriers significantly block the incoming flow, reducing the on-road air velocity and resulting in the difficult dispersion of vehicle emitted particles. Consequently, the dimensionless concentration of the particles in the on-road area reaches as high as 55 and the indoor particle concentrations are much lower than those with no barriers. It shows that reducing the on-road air velocity is a potential approach to constrain the vehicle emitted particles to the surrounding environment.

For the case of 90° wind direction and wind speed of 1 m/s, the noise barriers cannot effectively restrain the dispersion of vehicle emitted particles. Fig. 19 shows the airflow fields and corresponding particle concentration distributions on the plane of $x = 0$ m at two wind speeds of 4 m/s and 1 m/s in the wind direction of 90° , for the scenario of the noise barriers with windows open. It can be seen that a strong vortex is generated near the leeward side of noise barrier at the wind speed of 4 m/s, significantly restricts the dispersion of roadway particles toward downstream. On the contrary, relatively calm airflow pattern on the roadway is exhibited in the case of 1 m/s, without constraining the particle dispersion from large vortices. Therefore, the vehicle generated particles can travel a longer distance, resulting in higher indoor particle concentrations.

Similar to the noise barriers, the roadside canopies are expected to be effective in blocking the incoming flow and confining the particles to the on-road area, especially the dense canopy. Whereas, the roadside canopies can't abate the indoor particle concentrations. Moreover, in the wind direction of 90° and at the wind speed of 1 m/s, the indoor mean concentrations with roadside trees are much larger than those with no barriers as shown in Fig. 17(b). Fig. 20 can explain the reasons, in which two wind directions of 90° and 45° at the wind speed of 4 m/s with the dense trees on the roadsides are compared. The dense trees effectively block the incoming flow, leading to a lower air velocity in the on-road area than other zones, which is similar to the noise barriers. The transport of particles, yet, is more powerful in this

case, which can attribute to the gaps between the canopy elements and between the trees. Instead of being confined to the on-road area, the particles carried by the airflow penetrate through the dense canopy and transport downstream. Moreover, the particles captured by the surfaces inside the canopies are too few to effectively reduce the particle concentrations. Additionally, the concentration in the on-road zone is much smaller than that with the noise barriers, due to the penetration of particles as shown in Fig. 19.

Besides the dense canopies, the sparse roadside trees also cannot effectively reduce indoor particle concentrations especially at the lower wind speed as shown in Fig. 17. Furthermore, the sparse canopies are inferior to the dense one in the wind direction of 90° , while the difference becomes small in the wind direction of 45° because the tree canopies primarily impede air from passing in the wind direction of 90° . In this situation, the dense canopy having less cracks and gaps will significantly slow down the air velocity. However, the air penetrates more easily for the sparse one that more particles will transport downstream. On the other hand, in the 45° wind direction the tree canopies not only block the incoming flow but also act as a channel to lead air downstream, which weakens the particle penetration through the gaps within the canopy, so the sparse canopy plays a similar role to the dense one in the inflow direction of 45° .

The trees in front of the building are also regarded as a feasible way to mitigate the particle pollution near the roadway. Two positions of 10 m and 20 m away from the building facade, and two kinds of LAD distributions are taken into account. In the wind direction of 90° , the particle concentrations vary widely with the tree positions and LAD distributions, while the concentrations profiles are almost same in the direction of 45° . Fig. 21 shows the airflow fields on the plane of $x = 0$ m for the densely planted trees with two positions of 10 m and 20 m at the wind speed of 4 m/s in the wind direction 90° . The obstruction of the trees slows down the air velocity, and a large vortex analogous to the case of no barriers is generated in front of the building with a conspicuously lower vortex intensity, which will lead to the particle accumulation and severe indoor pollution. Fig. 21(b) shows that the air

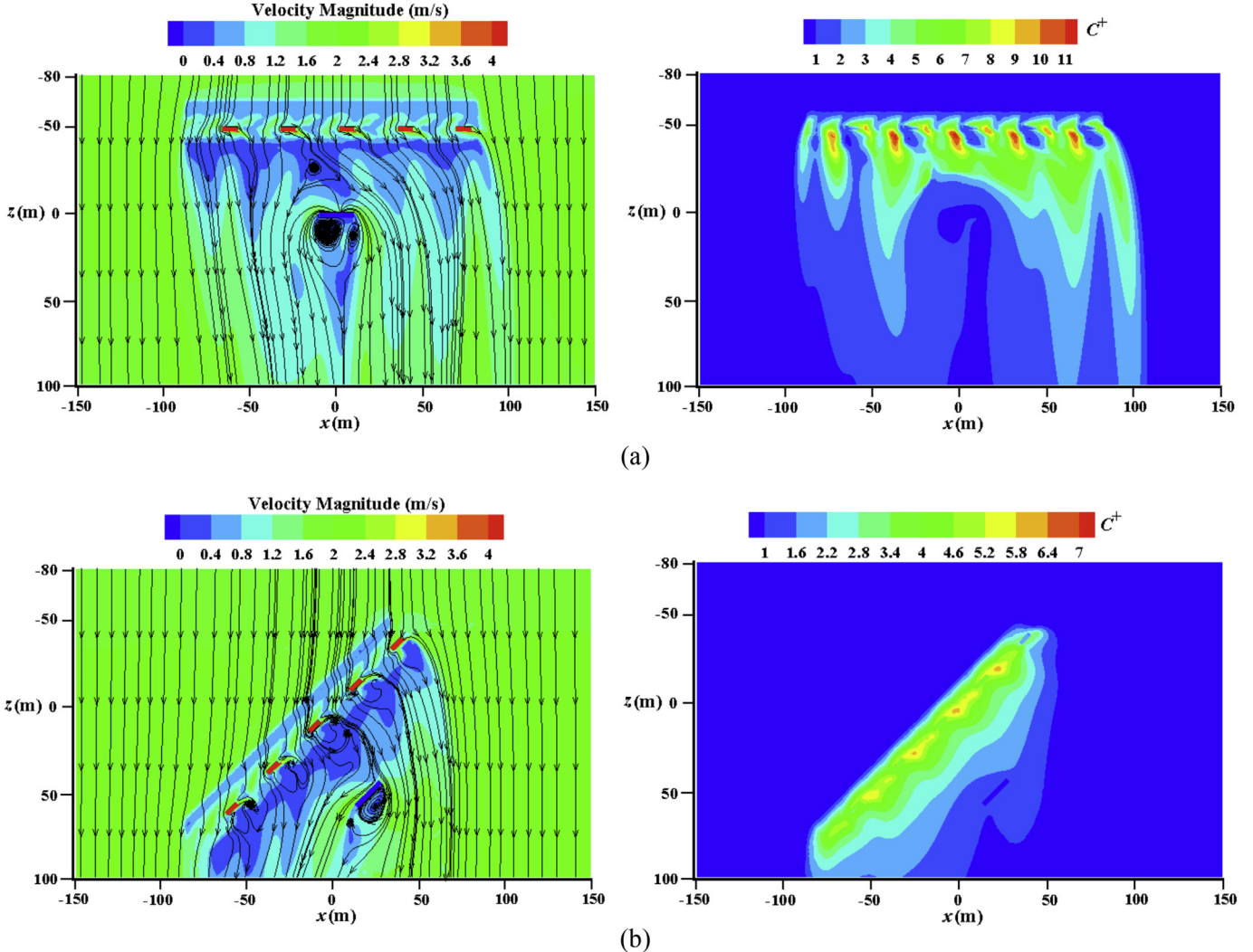


Fig. 20. Airflow fields and particle concentration distributions on the plane of $y = 3$ m in two wind directions of (a) 90° and (b) 45° at the wind speed 4 m/s, for the scenario of the dense trees on the roadsides with windows open.

velocity and vortex intensity for the case of 20 m away from the facade are smaller than the case of 10 m, resulting in a serious particle gathering and a higher indoor particle concentration as shown in Fig. 17(a). However, the effect of the tree positions is more complex at the wind speed of 1 m/s in the wind direction of

90° as shown in Fig. 17(b). In Fig. 22 the airflow fields on the plane of $x = 0$ m for two positions of 10 m and 20 m of the dense trees with the wind speed of 1 m/s and 90° inflow direction are given. Due to the obstruction of the trees, a vortex forms in front of the building and the center of the vortex is close to the third floor. For

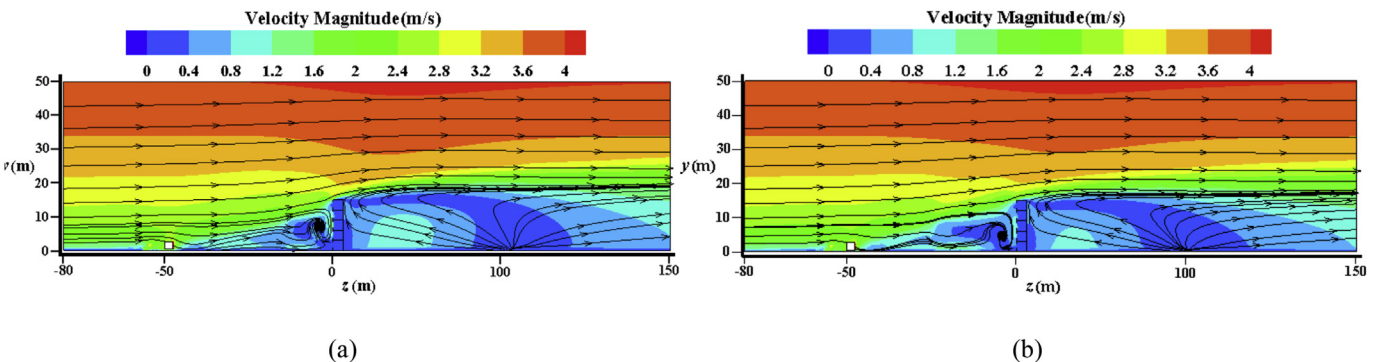


Fig. 21. Comparison of airflow fields on the plane of $x = 0$ m for the barriers of dense trees with two positions of (a) 10 m and (b) 20 m in front of the building facade, in the wind direction of 90° and at the wind speed of 4 m/s.

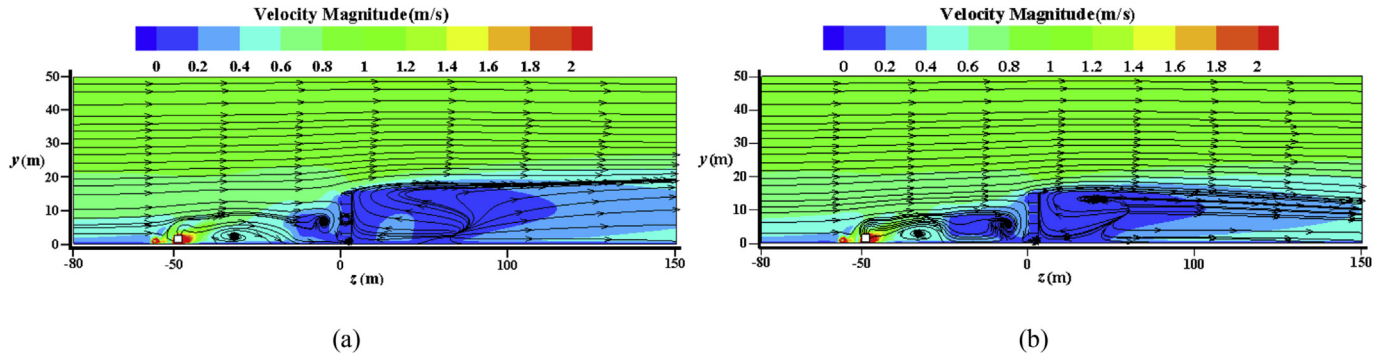


Fig. 22. Comparison of airflow fields on the plane of $x = 0$ m for the barriers of dense trees with two positions of (a) 10 m and (b) 20 m in front of the building facade, in the wind direction of 90° and at the wind speed of 1 m/s.

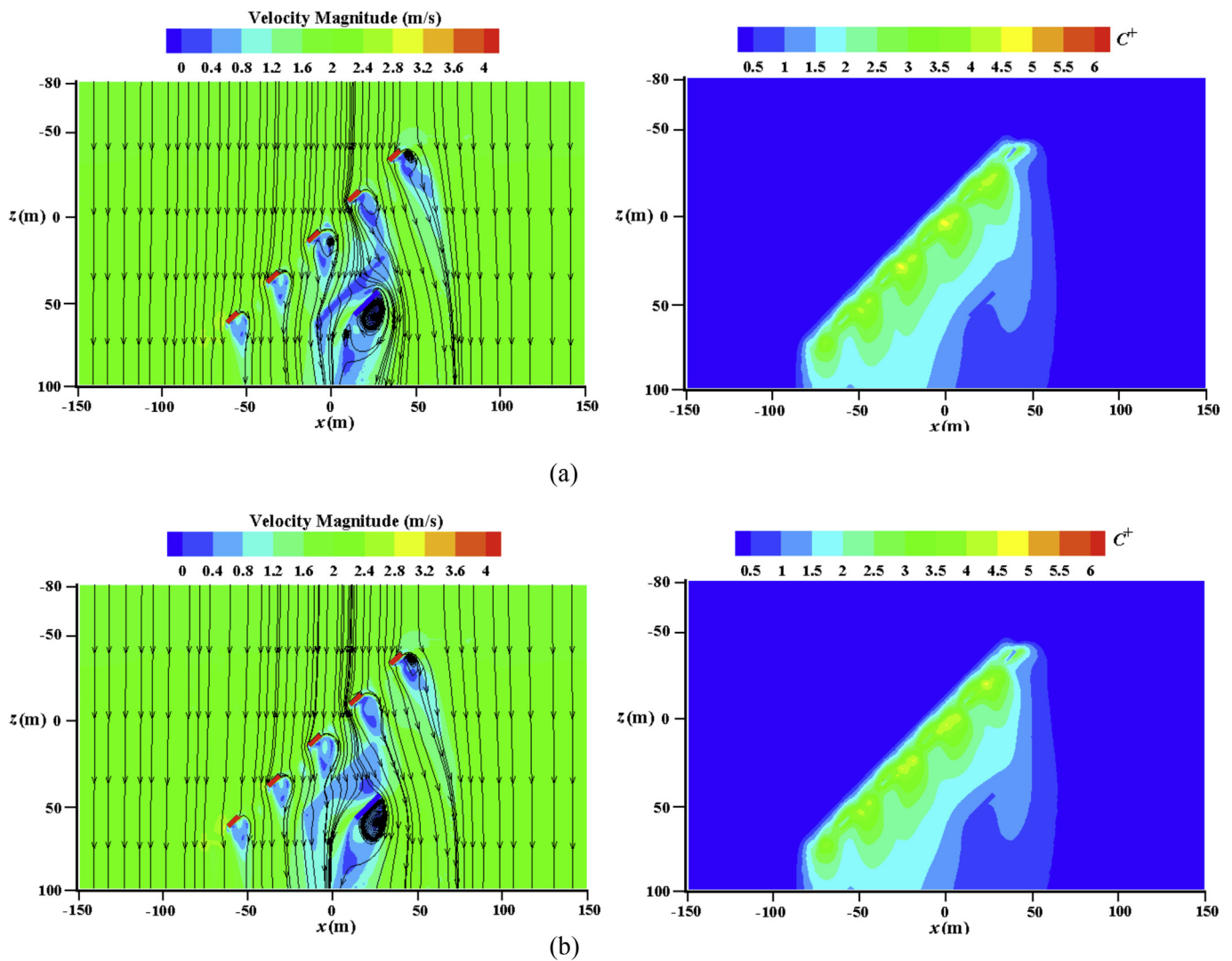


Fig. 23. Airflow fields and corresponding particle concentration distributions on the plane of $y = 3$ m for two kinds of barriers of (a) dense trees 10 m away from the facade and (b) sparse trees 20 m away from the facade, in the 45° incoming flow direction and at the wind speed of 4 m/s with windows open.

the lower floors, the vortex intensity for the case of 10 m is smaller than that of 20 m, facilitating more particles enter into the rooms. While the air velocity near the higher floors for the case of 10 m are larger than that of 20 m, which leads to a better ventilation effect. As for the effect of LAD distribution, no conspicuous

difference of concentration profiles between the dense and sparse canopies is found.

Fig. 23 shows the airflow patterns and corresponding concentration distributions on the plane of $y = 3$ m for two cases in the wind direction of 45° and at the wind speed of 4 m/s, first of which

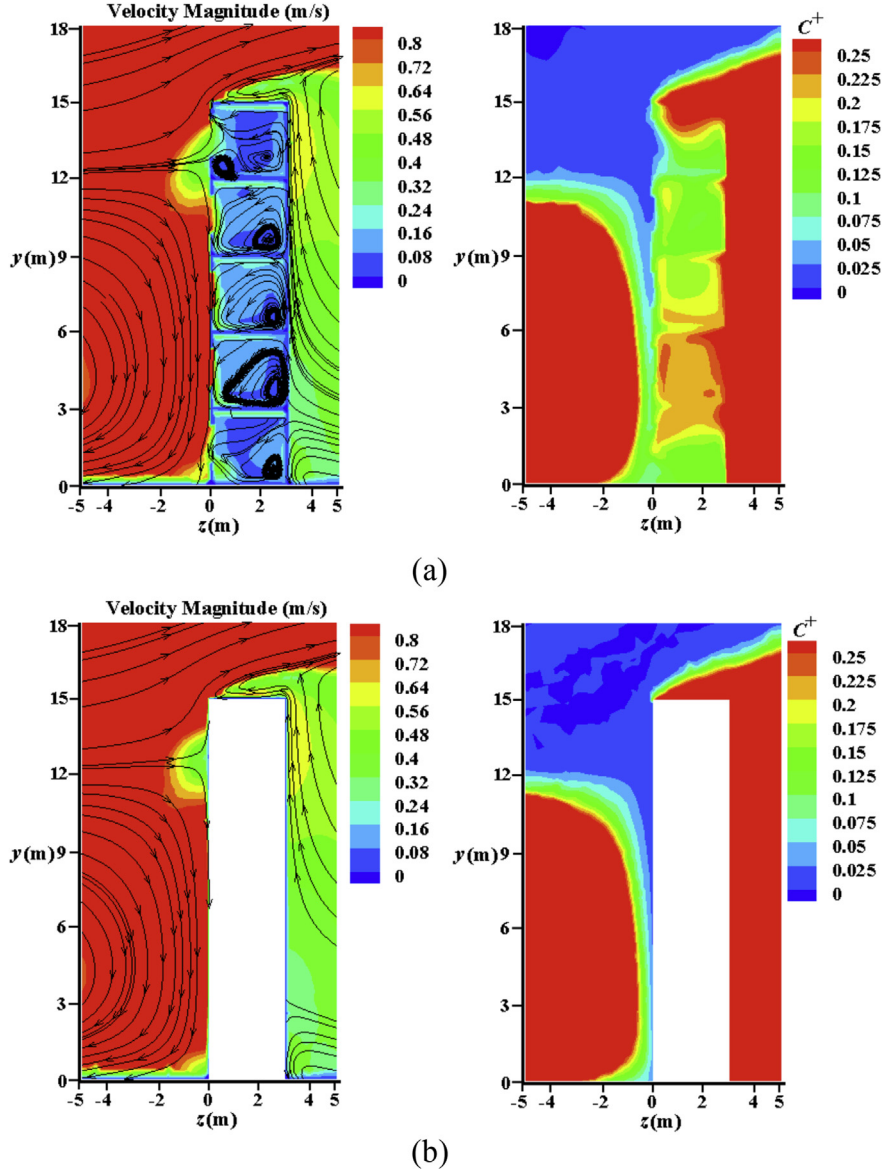


Fig. 24. Velocity and corresponding particle concentration fields on the plane of $x = 0$ m for the case of no barriers with (a) windows open and (b) windows closed, in 90° inflow direction and at wind speed of 4 m/s.

is the densely planted trees 10 m away from the building facade, and second is the sparsely planted trees 20 m away. It can be observed that the differences in the positions and LAD distributions of the trees have not lead to remarkable changes in the concentration profiles as indicated in Fig. 17(c) in the wind direction of 45° . In this case, the space between the trees and the road could act as a channel, leading the air to downstream and resulting in the dispersion of vehicle emitted particles along the channel, while the channel effect is not sensitive to the positions and LAD distributions of trees.

Based on the results with windows open, the noise barriers are the best choice in reducing the transport of the vehicle emitted particles to the indoor environment. The trees on the roadsides, no matter dense or sparse, cannot confine the particles on the road to achieve a low indoor particle concentration. As for the trees in front of the building, it is possible to reduce the indoor particle concentrations at low wind speeds in the oblique wind directions. In many meteorological conditions, however, the trees near the

building facade tend to accumulate airborne particles and increase the indoor particle concentrations.

3.4. Particle transport characteristics with windows closed

Based on the scenarios with windows closed, the particle transport characteristics are also investigated. For the 90° incoming flow and wind speed of 4 m/s, Fig. 24 gives the velocity and particle concentration fields on the plane of $x = 0$ m for the cases of no barriers with windows open and closed. When the windows are open, the outdoor airborne particles will directly enter into the room and result in indoor air pollution. While the outdoor particles can only enter into the room by infiltration process and most particles are blocked outside by the windows if the windows are closed.

The indoor particle concentration profiles with windows closed for eight kinds of barriers at two wind speeds in two wind directions are shown in Fig. 25. Generally, keeping the windows

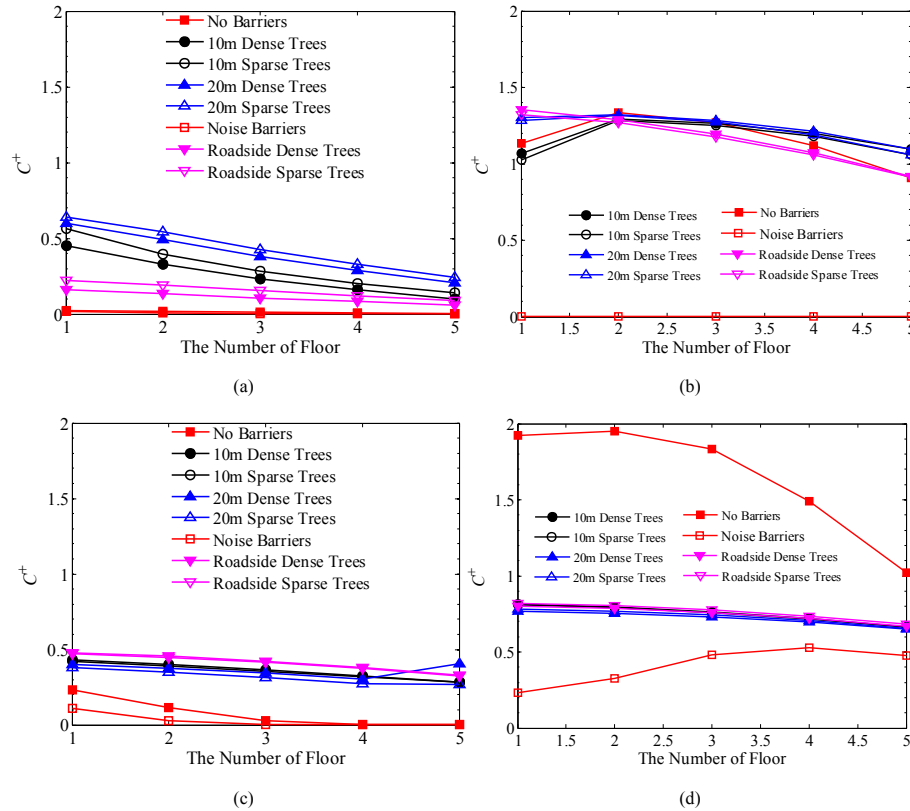


Fig. 25. Indoor particle concentration profiles with windows closed for eight kinds of barriers under different wind directions and speeds. (a) 90° inflow and 4 m/s wind speed, (b) 90° inflow and 1 m/s wind speed, (c) 45° inflow and 4 m/s wind speed, and (d) 45° inflow and 1 m/s wind speed.

Table 1

Deposition fluxes of 10 μm particles on the trees with windows open (unit in m/s).

| Cases | Deposition flux on the trees | | | | | | | | Roadside dense | | Roadside sparse | |
|----------------|------------------------------|------------|-------------|------------|------------|------------|-------------|------------|----------------|------------|-----------------|------------|
| | 10 m dense | | 10 m sparse | | 20 m dense | | 20 m sparse | | Upstream | Downstream | Upstream | Downstream |
| | Upstream | Downstream | Upstream | Downstream | Upstream | Downstream | Upstream | Downstream | Upstream | Downstream | Upstream | Downstream |
| 90°-4 m/s-open | 4.91e-03 | 5.01e-03 | 4.20e-03 | 4.34e-03 | 5.40e-06 | 9.78e-03 | 2.20e-06 | 8.48e-03 | | | | |
| 90°-1 m/s-open | 8.61e-03 | 8.93e-03 | 9.70e-03 | 9.76e-03 | 7.82e-06 | 2.29e-02 | 2.02e-05 | 2.44e-02 | | | | |
| 45°-4 m/s-open | 3.66e-03 | 3.66e-03 | 4.26e-03 | 4.26e-03 | 4.67e-04 | 7.90e-03 | 3.57e-04 | 7.42e-03 | | | | |
| 45°-1 m/s-open | 6.24e-03 | 6.34e-03 | 7.52e-03 | 7.61e-03 | 4.84e-03 | 1.20e-02 | 4.43e-03 | 1.21e-02 | | | | |

Table 2

Deposition percentages of 10 μm particles on the trees with windows open.

| Cases | Deposition percentage on the trees | | | | | | | | Roadside dense | | Roadside sparse | |
|----------------|------------------------------------|------------|----------|------------|-------------|------------|----------|------------|----------------|------------|-----------------|------------|
| | 10 m dense | | | | 20 m sparse | | | | Upstream | Downstream | Upstream | Downstream |
| | Upstream | Downstream | Upstream | Downstream | Upstream | Downstream | Upstream | Downstream | Upstream | Downstream | Upstream | Downstream |
| 90°-4 m/s-open | 0.42% | 0.30% | 0.39% | 0.28% | 0.42% | 0.71% | 0.27% | 0.44% | | | | |
| 90°-1 m/s-open | 1.61% | 1.14% | 1.55% | 1.11% | 1.57% | 2.97% | 1.07% | 1.83% | | | | |
| 45°-4 m/s-open | 0.58% | 0.39% | 0.53% | 0.36% | 0.48% | 1.03% | 0.29% | 0.68% | | | | |
| 45°-1 m/s-open | 2.46% | 1.78% | 2.62% | 1.86% | 1.83% | 4.17% | 1.13% | 2.82% | | | | |

closed can effectively reduce the indoor particle concentrations. Whereas, the concentration profiles present similar changing trends to those with windows open as shown in Fig. 17. The noise barriers effectively block the dispersion of the particles, leading to the lower indoor particle concentrations. While the roadside trees, no matter in dense or sparse form, cannot perform as effectively as the noise barriers. In addition, the positions and LAD distributions for the trees in front of the building play relatively important roles

in the wind direction of 90°, yet, the influences become lower in the wind direction of 45°. The changing of the indoor particle concentrations with windows closed differ conspicuously from that with windows open in the wind direction of 90° and at the wind speed of 1 m/s as shown in Fig. 25(b) and Fig. 17(b). When the windows are open, the indoor particle concentrations vary widely with the barriers, however, they are similar to each other even with different barriers as windows closed.

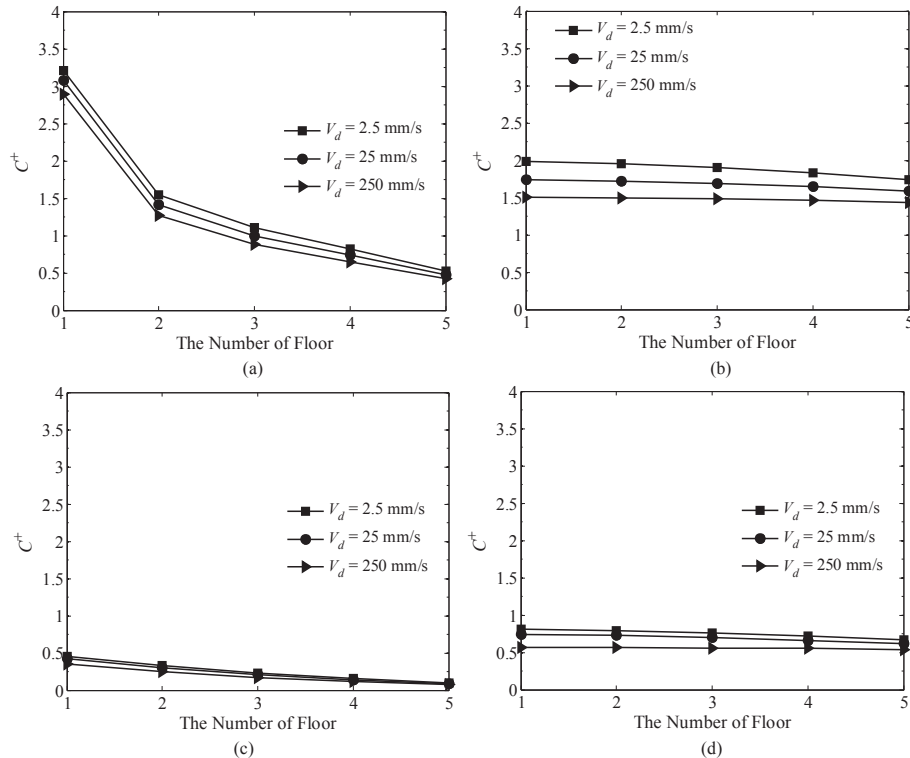


Fig. 26. Indoor particle concentration profiles at various deposition velocities for four cases with dense trees 10 m away from the building façade. (a) 90°, 4 m/s with windows open, (b) 45°, 1 m/s with windows open, (c) 90°, 4 m/s with windows closed and (d) 45°, 1 m/s with windows closed.

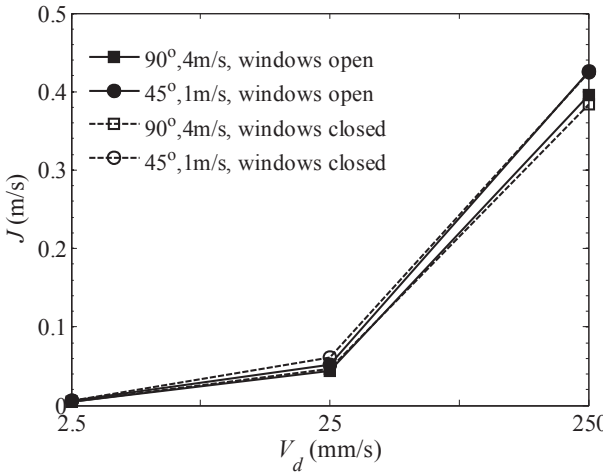


Fig. 27. Deposition fluxes on the trees for the four cases.

3.5. Comparison of particle deposition fluxes

The deposition fluxes of the particles with the diameter of 10 μm on the trees in two wind directions and at two wind speeds with the windows open are listed in Table 1. At the low wind speed, more airborne particles tend to accumulate inside the tree canopies, producing the relatively high deposition fluxes. While the deposition fluxes vary little with the LAD distributions of the trees. In addition, the deposition fluxes do not present a big difference between the two tree positions, namely 10 m and 20 m away from the facade. For the roadside trees, the deposition flux on the upstream canopy is significantly smaller than that of the downstream one. As

shown in Fig. 20, the particle concentrations near the downstream canopies of the roadside are higher than those near the upstream, which will generate higher deposition fluxes.

When penetrating into the canopies, the particles will be captured by the vegetative elements or transport outside by the air flow. Similar to the deposition flux, the flux of particles advected by air is defined as $J_{a,i} = v \times C_i$ where v is the air velocity inside the canopy. Then the deposition percentage including the resuspension effect is calculated as $P_{deposition,i} = J_{d,i} \times P_{resuspension} / (J_{d,i} \times P_{resuspension} + J_{a,i})$. Table 2 lists the deposition percentages of 10 μm particles on the trees with windows open. The larger deposition percentages appear at the cases of smaller wind speed, 1 m/s, and more particles tend to accumulate inside the canopy, facilitating the deposition process. In addition, larger percentages are generated in the direction of 45° at the same wind speed. However, the difference in different wind directions is reduced as the wind speed increases. Moreover, the denser canopies produce larger deposition percentages than the sparser ones, showing a better capture effect. From Table 2, it can also be seen that the maximum deposition percentage is less than 5%, showing that the particles captured by the surfaces inside the canopies are too few to effectively reduce their concentrations.

3.6. Influence of particle deposition velocity

It is well known that the tree canopies can intercept the airborne particles, and in many investigations the particle deposition process is taken into account by using the term of deposition velocity. In this study, the particle deposition velocity is set 2.5 mm/s for the category of 10 μm according to the model of Zhang et al. [32]. Two more velocities of 25 mm/s and 250 mm/s, respectively 10 and 100 times of the model value are also studied to clarify the effect of the deposition velocity on the particle transport

characteristics. The indoor particle concentrations for four cases with dense trees 10 m away from the building facade are shown in Fig. 26. It can be seen that increasing the particle deposition velocity is able to reduce the indoor particle concentrations, and nearly 30% concentration drops are observed when the deposition velocity reaches 250 mm/s. The corresponding deposition fluxes on the trees for the four cases are shown in Fig. 27, from which can be seen that the deposition flux at the deposition velocity of 250 mm/s is approximately 40 times higher than that at the deposition velocity of 2.5 mm/s. Although other cases are not demonstrated here, similar trends at the three deposition velocities are also achieved, showing that the indoor particle concentrations can be restrained to a great extent by increasing the particle deposition velocity. Some species with dense villi and relatively coarse blades tend to have higher deposition velocities, so the particles can be easily captured. City designers may choose these species to mitigate the air pollution near the roadway.

4. Conclusions

The drift-flux model combined with the dry deposition model and Eulerian fluid methods have been employed to predict the particle transport characteristics in the micro-environment near the roadway. Eight kinds of barriers with two wind directions, two wind speeds and two window states, totally 192 cases have been investigated.

The wind speed plays a significant role in the dispersion of the vehicle emitted particles. The higher the wind speed is, the lower the indoor particle concentration exhibits. Among eight kinds of barriers, the noise barriers can effectively block the incoming flow and restrain the vehicle emitted particles from transporting downstream under most of the meteorological conditions. The vegetation canopies along the roadsides cannot confine the particle dispersion, however, the trees in front of the building facade tend to slow down the air velocity and result in particle gathering near the windows, leading to higher indoor particle concentrations. The indoor particle concentrations vary widely with the positions and LAD distributions of the trees in the wind direction of 90°, yet, almost remain unchanged in the wind direction of 45°. The indoor particle concentrations can be reduced by increasing the particle deposition velocity on trees and keeping the windows closed.

Acknowledgments

The financial supports for this research, from the National Natural Science Foundation of China (Grant No. 51476055) and the National Basic Research Program of China (Grant No. 2015CB251503), are gratefully acknowledged.

References

- [1] D.W. Dockery, C.A. Pope, X. Xu, J.D. Spengler, J.H. Ware, M.E. Fay, B.G. Ferris, F.E. Speizer, An association between air pollution and mortality in six U.S. Cities, *N. Engl. J. Med.* 329 (1993) 1753–1759.
- [2] Y.Y. Chen, A. Ebenstein, M. Greenstone, H.B. Li, Evidence on the impact of sustained exposure to air pollution on life expectancy from China's Huai River policy, *PNAS* 110 (2013) 12936–12941.
- [3] W.W. Nazaroff, Indoor particle dynamics, *Indoor Air* 14 (2004) 175–183.
- [4] K.M. Zhang, A.S. Wexler, Evolution of particle number distribution near roadways—Part I: analysis of aerosol dynamics and its implications for engine emission measurement, *Atmos. Environ.* 38 (2004) 6643–6653.
- [5] K.M. Zhang, A.S. Wexler, Y.F. Zhu, W.C. Hinds, C. Sioutas, Evolution of particle number distribution near roadways. Part II: the 'Road-to-Ambient' process, *Atmos. Environ.* 38 (2004) 6655–6665.
- [6] Y.J. Wang, K.M. Zhang, Modeling near-road air quality using a computational fluid dynamics model, CFD-VIT-RIT, *Environ. Sci. Technol.* 43 (2009) 7778–7783.
- [7] J.T. Steffens, Y.J. Wang, K.M. Zhang, Exploration of effects of a vegetation barrier on particle size distributions in a near-road environment, *Atmos. Environ.* 50 (2012) 120–128.
- [8] B.A. Maher, I.A.M. Ahmed, B. Davison, V. Karloukovski, R. Clarke, Impact of roadside tree lines on indoor concentrations of traffic-derived particulate matter, *Environ. Sci. Technol.* 47 (2013) 13737–13744.
- [9] J.T. Steffens, D.K. Heist, S.G. Perry, K.M. Zhang, Modeling the effects of a solid barrier on pollutant dispersion under various atmospheric stability conditions, *Atmos. Environ.* 69 (2013) 76–85.
- [10] P.E.J. Vos, B. Maiheu, J. Vankerkom, S. Janssen, Improving local air quality in cities: to tree or not to tree? *Environ. Pollut.* 183 (2013) 113–122.
- [11] A. Wania, M. Bruse, N. Blond, C. Weber, Analysing the influence of different street vegetation on traffic-induced particle dispersion using microscale simulations, *J. Environ. Manage.* 94 (2012) 91–101.
- [12] A.N. Al-Dabbous, P. Kumar, The influence of roadside vegetation barriers on airborne nanoparticles and pedestrians exposure under varying wind conditions, *Atmos. Environ.* 90 (2014) 113–124.
- [13] R. Buccolieri, S.M. Salim, L.S. Leo, S.D. Sabatino, A. Chan, P. Ielpo, G.D. Gennaro, C. Gromke, Analysis of local scale tree-atmosphere interaction on pollutant concentration in idealized street canyons and application to a real urban junction, *Atmos. Environ.* 45 (2011) 1702–1713.
- [14] M. Tallis, G. Taylor, D. Sinnott, P. Freer-Smith, Estimating the removal of atmospheric particulate pollution by the urban tree canopy of London, under current and future environments, *Landscape Urban Plan.* 103 (2011) 129–138.
- [15] D.E. Pataki, M.M. Carreiro, J. Cherrier, N.E. Grulke, V. Jennings, S. Pincetl, R.V. Pouyat, T.H. Whitlow, W.C. Zipperer, Coupling biogeochemical cycles in urban environments: ecosystem services, green solutions, and misconceptions, *Front. Ecol. Environ.* 9 (2011) 27–36.
- [16] M. Bruse, H. Fleer, Simulating surface-plant-air interactions inside urban environments with a three dimensional numerical model, *Environ. Model. Softw.* 13 (1998) 373–384.
- [17] B.E. Launder, D.B. Spalding, The numerical computation of turbulence flows, *Comput. Methods Appl. Mech. Eng.* 3 (1974) 269.
- [18] B. Zhao, Y. Zhang, X.T. Li, X.D. Yang, D.T. Huang, Comparison of indoor aerosol particle concentration and deposition in different ventilated rooms by numerical method, *Build. Environ.* 39 (2004) 1–8.
- [19] Ansys, Inc, ANSYS FLUENT Theory Guide, ANSYS Inc., Canonsburg, PA, 2010.
- [20] R. Buccolieri, C. Gromke, S.D. Sabatino, B. Ruck, Aerodynamic effects of trees on pollutant concentration in street canyons, *Sci. Total Environ.* 407 (2009) 5247–5256.
- [21] J.L. Santiago, F. Martín, A. Cuerva, N. Bezdenejnykh, A. Sanz-Andrés, Experimental and numerical study of wind flow behind windbreaks, *Atmos. Environ.* 41 (2007) 6406–6420.
- [22] J.D. Wilson, Oblique, stratified winds about a shelter fence. Part I: measurements, *J. Appl. Meteorol.* 43 (2004) 1149–1167.
- [23] A.S. Thom, Momentum, mass and heat-exchange of vegetation, *Q. J. R. Meteorol. Soc.* 98 (1972) 124–134.
- [24] J.C. Kaimal, J.J. Finnigan, *Atmospheric Boundary Layer Flows: Their Structure and Measurement*, Oxford University Press, 1994.
- [25] S.R. Green, Modelling turbulent air flow in a stand of widely-spaced trees, *Phoenics J. Comput. Fluid Dyn. Appl.* 5 (1992) 294–312.
- [26] J.H. Amorim, V. Rodrigues, R. Tavares, J. Valente, C. Borrego, CFD modelling of the aerodynamic effect of trees on urban air pollution dispersion, *Sci. Total Environ.* 461–462 (2013) 541–551.
- [27] F.Z. Chen, S.C.M. Yu, A.C.K. Lai, Modeling particle distribution and deposition in indoor environments with a new drift-flux model, *Atmos. Environ.* 40 (2006) 357–367.
- [28] A.C.K. Lai, W.W. Nazaroff, Modeling indoor particle deposition from turbulent flow onto smooth surfaces, *J. Aerosol Sci.* 31 (2000) 463–476.
- [29] M.Z. Jacobson, *Fundamentals of Atmospheric Modeling*, second ed., Cambridge University Press, 2005.
- [30] A. Petroff, A. Maillat, M. Amielha, F. Anselmet, Aerosol dry deposition on vegetative canopies. Part II: a new modelling approach and applications, *Atmos. Environ.* 42 (2008) 3654–3683.
- [31] A. Petroff, L.M. Zhang, S.C. Pryor, Y. Belot, An extended dry deposition model for aerosols onto broadleaf canopies, *J. Aerosol Sci.* 40 (2009) 218–240.
- [32] L.M. Zhang, S.L. Gong, J. Padro, L. Barrie, A size-segregated particle dry deposition scheme for an atmospheric aerosol module, *Atmos. Environ.* 35 (2001) 549–560.
- [33] D. Nowak, S. Hirabayashi, A. Bodine, R. Hoehn, Modeled PM2.5 removal by trees in ten U.S. cities and associated health effects, *Environ. Pollut.* 178 (2013) 395–402.
- [34] Y. Jiang, D. Alexander, H. Jenkins, R. Arthur, Q.Y. Chen, Natural ventilation in buildings: measurement in a wind tunnel and numerical simulation with large-eddy simulation, *J. Wind Eng. Ind. Aerodyn.* 91 (2003) 331–353.
- [35] Y.L. Li, D.C. Zhang, X.M. Jin, L.J. Yang, X.Z. Du, Y.P. Yang, Transportation characteristics of motor vehicle pollutants near Beijing typical expressway, *Sci. China Technol. S. C.* 59 (2016) 468–475, <http://dx.doi.org/10.1007/s11431-015-5997-7>.
- [36] COST Action 732. Quality assurance and improvement of micro-scale meteorological models. Available at: <http://www.mi.uni-hamburg.de/Home.4840.html>.
- [37] T.H. Whitlow, A. Hall, K.M. Zhang, J. Anguita, Impact of local traffic exclusion on near-road air quality: findings from the New York City "Summer Streets" campaign, *Environ. Pollut.* 159 (2011) 2016–2027.
- [38] U. Uhrner, S.V. Löwisch, H. Vehkämäki, B. Wehnert, S. Bräsel, M. Hermann, F. Stratmann, M. Kulmala, A. Wiedensohler, Dilution and aerosol dynamics

- within a diesel car exhaust plume-CFD simulations of on-road measurement conditions, *Atmos. Environ.* 41 (2007) 7440–7461.
- [39] D. Etheridge, M. Sandberg, *Building Ventilation: Theory and Measurement*, Wiley, Chichester, UK, 1996.
- [40] N.P. Gao, J.L. Niu, M. Perino, P. Heiselberg, The airborne transmission of infection between flats in high-rise residential buildings: tracer gas simulation, *Build. Environ.* 43 (2008) 1805–1817.
- [41] X.M. Jin, L.J. Yang, X.Z. Du, Y.P. Yang, Numerical investigation of particle transport characteristics in an isolated room with single-sided natural ventilation, *Build. Simul.* 9 (2016) 43–52.
- [42] N.P. Gao, J.L. Niu, M. Perino, P. Heiselberg, The airborne transmission of infection between flats in high-rise residential buildings: particle simulation, *Build. Environ.* 44 (2009) 402–410.
- [43] X.B. Shen, Z.L. Yao, H. Huo, K.B. He, Y.Z. Zhang, H. Liu, Y. Ye, PM_{2.5} emissions from light-duty gasoline vehicles in Beijing, China, *Sci. Total Environ.* 487 (2014) 521–527.
- [44] C. Gromke, R. Buccolieri, S.D. Sabatino, B. Ruck, Dispersion study in a street canyon with tree planting by means of wind tunnel and numerical investigations- evaluation of CFD data with experimental data, *Atmos. Environ.* 42 (2008) 8640–8650.
- [45] B. Lalic, D.T. Mihailovic, An empirical relation describing leaf-area density inside the forest for environmental modeling, *J. Appl. Meteorol.* 43 (2004) 641–645.
- [46] C. Chen, B. Zhao, Review of relationship between indoor and outdoor particles: I/O ratio, infiltration factor and penetration factor, *Atmos. Environ.* 45 (2011) 275–288.
- [47] J. Kearney, L. Wallace, M. MacNeill, M. Héroux, W. Kindzierski, A. Wheeler, Residential infiltration of fine and ultrafine particles in Edmonton, *Atmos. Environ.* 94 (2014) 793–805.
- [48] J. Hitchins, L. Morawska, D. Gilbert, M. Jamriska, Dispersion of particles from vehicle emissions around high- and low-rise buildings, *Indoor Air* 12 (2002) 64–71.